Addressing the $N\Omega$ femtoscopy correlation function using baryon-baryon effective potentials

Master's thesis

Marc Piquer i Méndez

Advisors: Dr. Assumpta Parreño García,
Dr. Juan Torres-Rincon.

UNIVERSITAT DE BARCELONA

UNIVERSIDAD D SEVILLA 1505

12 July 2024

Abstract

We have generated an updated version of the $N\Omega$ potential for low-energy interactions based on an effective field theory approach at leading order, fitting the parameters to match a known lattice QCD potential for the ${}^5S_2 \to {}^5S_2$ channel. This potential, other potentials based on different parametrizations and the mentioned lattice QCD potential have been used to solve the Schrödinger equation numerically, obtaining the scattering wave functions for different values of the relative momentum. Using these wave functions, we have computed the $N\Omega$ femtoscopic correlation functions and compared the results for the $\mathrm{p}\Omega$ case with those published by the ALICE collaboration. Additionally, bound states for the potential are predicted not only for the ${}^5S_2$ state but also for the ${}^3S_1$ state.

Acknowledgements

I want to express my gratitude to my advisors, Assumpta Parreño García and Juan Torres-Rincon, for their pacience and good counseling throughout the whole academic course. Their level of dedication has been much higher than what I could have ever asked for. I also want to thank them for suggesting the topic of this work, about which I did not have any previous knowledge and which has proven to be very interesting to study.

In this difficult year, I also want to thank my family for their support through my whole academic life. Even when they had doubts, they have always supported my decisions and provided me with the best education possible.

An acknowledgement is in order also for my friends. As always, I am grateful to those who have always been there and who I know I can always count on. A special thanks goes this time to the friends who have assisted me in completing this work, whose support has been crucial. This course, in particular, I also want to thank my colleagues from the master's degree: they have helped me a lot in my academic difficulties and made the whole experience much nicer.

Last, but not least, I want to thank the Institut de Ciències del Cosmos (ICCUB) for their financial support for this master's degree.

Contents

1 Introduction

In studying the hadron-hadron interaction, two fundamental interactions play an important role: the electromagnetic interaction and the strong interaction. The former is well understood and described by the Coulomb potential, whereas the latter is much more difficult to treat. The fundamental theory of the strong interaction, quantum chromodynamics (QCD), provides an accurate description of its behaviour at the quark and gluon scale, but it is challenging to obtain the baryon-baryon interaction from it.

While high energy phenomena may be described by a perturbative approach through asymptotic freedom, such technique does not work at the low energy baryon-baryon scale. At such regimes, the most well-known approach is to regularize the theory by formulating it in discrete spacetime, which naturally introduces a cut-off, and then extrapolating the results to null lattice spacing. This formulation is known as lattice QCD, and, while being computationally intensive, it has been known to give very accurate results.

Another common option to study QCD in the non-perturbative regime is to use what is known as an effective field theory (EFT). In this approach, we build an effective interaction which is adapted to the natural degrees of freedom of the system, the hadrons. For light baryons and mesons, one such method is chiral perturbation theory (χPT). In this theory, we describe the couplings through diagrams, which we organize according to their momentum chiral power ν using the Weinberg power counting formula [Wei90],

$$\nu = 2 + 2L - B + \sum_i V_i(d_i + b_i/2 - 2), \tag{1.1}$$

where L is the number of loops, B is the number of incoming baryon fields, and for the V_i vertices of type i there are d_i derivatives and b_i internal baryon lines. We call leading order (LO) the expansion up to $\nu = 0$.

As for the couplings in each diagram, we use a Lagrangian adapted to the relevant degrees of freedom and symmetries of the system. We will have different operational structures, each of which will appear in the Lagrangian with an associated low-energy constant. Then, we will use this Lagrangian to describe the diagrams' vertices.

Apart from hadrons made up of just up and down quarks, the lighter hadrons are those which contain at least one strange quark, called hyperons. Among them, due to its content, the heaviest is the isoscalar, $J^\pi = 3/2^+$, Ω baryon, consisting of three strange quarks. The interaction of this baryon with nucleons, the $N\Omega$ interaction, will be the focus of this work.

Hyperons are not stable, and they decay in free space mainly through weak interaction processes. Nevertheless, bound systems of nucleons and one (or even more) hyperon can be experimentally produced [SD+21] with lifetimes around 10^{-10} s. Adding one or more hyperons to a nucleus generally shrinks its size, in a "glue-like" effect. For instance, $N\Omega$ is a candidate for a dibaryon (that is, a bound state of two baryons). One of the interaction potentials, of which we will make extensive use, is the one resulting from a fit to a lattice QCD potential in the ${}^5S_2 \to {}^5S_2$ channel obtained by the HAL QCD collaboration [IA+19] which, as we shall see, does indeed allow for a bound state. However, it is important to note that said state has not been found experimentally so far.

As for the study of the interaction, the usual method for the hadron-hadron interaction uses scattering experiments. These experiments become more and more difficult when the involved particles are not stable, which is the case of the Ω baryon, since notable difficulties arise when preparing a particle beam. Hence, there is interest in following an alternative approach.

In this regard, the study of the femtoscopy correlation function has been found to give good results. The features of the interaction are mapped in the shape of a function of the relative momentum $C(\vec{k})$, which can also be obtained experimentally in certain collisions from [FMV21]

$$C_{\text{exp}}(\vec{k}) = \xi(\vec{k})\frac{N(\vec{k})}{N_{\text{ref}}(\vec{k})}, \tag{1.2}$$

where N is the momentum distribution of pairs produced in the same event, N_{ref} is the distribution

obtained combining particles produced in different collisions and ξ is a correction due to experimental effects.

Some interesting results have recently been obtained through this method by the ALICE collaboration using pp collisions [ALI20] and by the STAR collaboration using AuAu collisions [STA19].

The correlation function can be computed from the interaction using several methods. The one we will focus on consists in solving the Schrödinger equation numerically for a given potential and momentum $\vec{k}$ and then obtaining the value $C(\vec{k})$ at that point using the Koonin-Pratt formula

$$C(\vec{k}) = \int_{\mathbb{R}^3} S(\vec{r})|\psi(\vec{r},\vec{k})|^2 \,\mathrm{d}\vec{r}\,. \tag{1.3}$$

In the previous equation, ψ is the scattering wave function with momentum $\vec{k}$ and $S(\vec{r})$, known as source function, is a probability density function on $\mathbb{R}^3$ which models the hadron production and must, therefore, contain information on the geometry of the system. Since we will compare the $\mathrm{p}\Omega$ correlation function we obtain with the pp collision results from [ALI20], we will use the same source function used there, namely, a Gaussian with radius $r_0 = 0.95\ \mathrm{fm}$.

For the correlation function, therefore, we need the scattering wave functions. Since we are going to work with a potential with spherical symmetry, we will reduce the Schrödinger equation to the radial equation

$$\left[\frac{\mathrm{d}^2}{\mathrm{d}r^2} + k^2 - \frac{2\mu Z_1 Z_2 \alpha}{r} - 2\mu\hat{V}(r) - \frac{l(l+1)}{r^2}\right] u_l(r) = 0, \tag{1.4}$$

where u_l are the reduced radial wave functions, μ is the reduced mass of the system and Z_1, Z_2 are the charges of the particles. Solving this equation numerically will give us the input we need for the correlation function computation.

This calculation will consist in three parts: one where we derive and discuss different potentials, one where we compute the scattering wave functions from these potentials, and one where we compute the correlation functions. All of the numerical computations will be done with a Fortran 90 code.

Apart from the fundamental interest it raises, understanding the $N\Omega$ interaction is relevant to astrophysics, since hyperon-nucleon interactions may play an important role in neutron stars, as hyperons may be present in large enough amounts to affect their equation of state, for which we need to understand the interactions both among them and with nucleons [TF20].

All data plotted in the figures for this work can be found in the [Piq24] repository.

2 $N\Omega$ potential derivation within EFT

As commented, the first task we need to accomplish is obtaining an interaction potential for the $N\Omega$ interaction. We will proceed with an effective approach and will get its constants by fitting to the lattice QCD potential from [IA+19], which is computed for the ${}^5S_2 \to {}^5S_2$ interaction. Then, these constants will be used to study the other relevant channels.

2.1 Leading order $N\Omega$ diagrams

As we commented, when studying the $N\Omega$ interaction, we may organize the Feynman diagrams according to their chiral power ν, given by Weinberg's power counting (1.1). We will stick to the LO case, $\nu = 0$, given by the one meson exchange diagrams ($b_i = 2$, $d_i = 1$) and the contact terms ($b_i = 4$, $d_i = 0$).

2.1.1 One meson exchange diagrams

First, we will study the one meson exchange diagrams. In each of them, we label 1 the left side vertex and 2 the right side vertex. We write I_n and J_n (with $n \in \{1, 2\}$) for the final isospin and spin for the outgoing baryon from node n. The relevant physical properties the baryons and mesons participating in the diagrams are in table 1.

	p	n	Λ	Σ^+	Σ^0	Σ^-	Ξ^0	Ξ^-
Quark content	uud	udd	uds	uus	uds	dds	uss	dss
I	1/2	1/2	0	1	1	1	1/2	1/2

(a) Octet baryons ($J^\pi = 1/2^+$).

	Σ^{*+}	Σ^{*0}	Σ^{*-}	Ξ^{*0}	Ξ^{*-}	Ω^-
Quark content	uus	uds	dds	uss	dss	sss
I	1	1	1	1/2	1/2	0

(b) Decuplet baryons ($J^\pi = 3/2^+$) with non-zero strangeness.

	η	π^-	π^0	π^+	K^-	K^0	$\overline{\mathrm{K}^0}$	K^+
Quark content	$(\mathrm{u\bar{u}} + \mathrm{d\bar{d}} - 2\mathrm{s\bar{s}})/\sqrt{6}$	$\mathrm{d\bar{u}}$	$(\mathrm{u\bar{u}} - \mathrm{d\bar{d}})/\sqrt{2}$	$\mathrm{u\bar{d}}$	$\mathrm{s\bar{u}}$	$\mathrm{d\bar{s}}$	$\mathrm{s\bar{d}}$	$\mathrm{u\bar{s}}$
I	0	1	1	1	1/2	1/2	1/2	1/2

(c) Octet mesons ($J^\pi = 0^-$).

Table 1: Particle data we will need to analyze the diagrams.

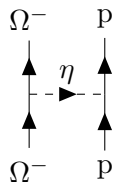

Figure 1: η meson exchange diagram.

The exchange of a η meson is the only one that fulfills conservation of isospin, charge and strangeness at each vertex of the diagram, depicted in figure 1.

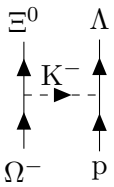

(a) $I_2 = 0$, $J_1 = J_2 = 1/2$.

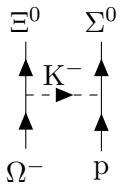

(b) $I_2 = 1$, $J_1 = J_2 = 1/2$.

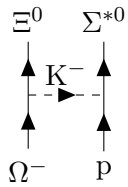

(c) $I_2 = 1$, $J_1 = 1/2$, $J_2 = 3/2$.

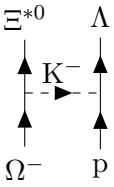

(d) $I_2 = 0$, $J_1 = 3/2$, $J_2 = 1/2$.

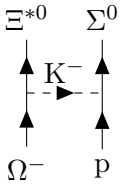

(e) $I_2 = 1$, $J_1 = 3/2$, $J_2 = 1/2$.

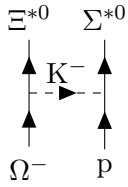

(f) $I_2 = 1$, $J_1 = J_2 = 3/2$.

Figure 2: K^- meson exchange cases. In all of them we get $I_1 = 1/2$.

The second case corresponds to the exchange of a K^- meson, which has quark content $\mathrm{s\bar{u}}$. This one is the meson forcefully, since, in node 1, we have $\Delta S_1 = \Delta Q_1 = 1$, which eliminates all other octet mesons. The different results arise from the different isospin and angular momentum couplings, which are written below each diagram.

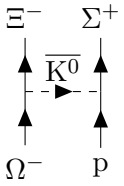

(a) $J_1 = J_2 = 1/2$.

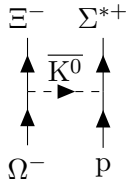

(b) $J_1 = 1/2$, $J_2 = 3/2$.

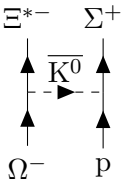

(c) $J_1 = 3/2$, $J_2 = 1/2$.

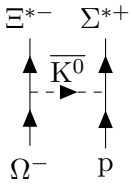

(d) $J_1 = J_2 = 3/2$.

Figure 3: $\overline{\mathrm{K}^0}$ meson exchange cases. In all of them we get $I_1 = 1/2$, $I_2 = 1$.

The third case correspond to the exchange of the $\overline{\mathrm{K}^0}$ meson, which has quark content $\mathrm{s\bar{d}}$. It needs to be this one meson due to the fact that, in node 1, we have $\Delta S_1 = 1$, $\Delta Q_1 = 0$, which eliminates all other octet mesons.

The quark content of a p baryon (a proton) is uud, whereas the quark content of Ω^- is sss. In a one meson exchange model, the resulting states may exchange at most one quark, depending on the meson, which ensures that we have written all possible diagrams. The same reasoning is valid for the neutron case below.

The only difference in the neutron case is due to the fact that the quark content of n is udd, so the resulting states (and the exchanged mesons) will have different quark content.

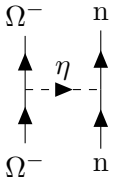

Figure 4: η meson exchange diagram.

The first case is identical to the proton one: it is the η meson exchange, which preserves both baryons.

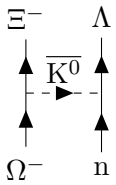

(a) $I_2 = 0$, $J_1 = J_2 = 1/2$.

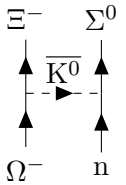

(b) $I_2 = 1$, $J_1 = J_2 = 1/2$.

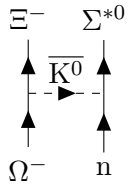

(c) $I_2 = 1$, $J_1 = 1/1$, $J_2 = 3/2$.

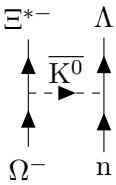

(d) $I_2 = 0$, $J_1 = 3/2$, $J_2 = 1/2$.

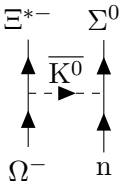

(e) $I_2 = 1$, $J_1 = 3/2$, $J_2 = 1/2$.

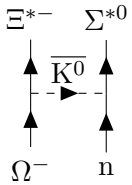

(f) $I_2 = 1$, $J_1 = J_2 = 3/2$.

Figure 5: $\overline{\mathrm{K}^0}$ meson exchange cases. In all of them we get $I_1 = 1/2$.

The second case now corresponds to the exchange of a $\overline{\mathrm{K}^0}$ meson, which has quark content $\mathrm{s\bar{d}}$. These and the next are swapped from the proton case due to the one quark difference appearing in all of the products.

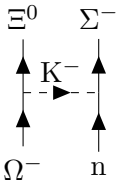

(a) $J_1 = J_2 = 1/2$.

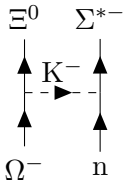

(b) $J_1 = 1/2$, $J_2 = 3/2$.

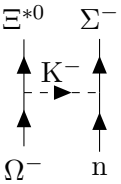

(c) $J_1 = 3/2$, $J_2 = 1/2$.

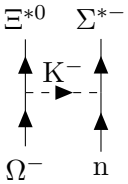

(d) $J_1 = 3/2$, $J_2 = 3/2$.

Figure 6: K^- meson exchange cases. In all of them we get $I_1 = 1/2$, $I_2 = 1$.

The third case corresponds to the exchange of a K^- meson, which has quark content $\mathrm{s\bar{u}}$.

2.1.2 Contact terms

As we discussed in the previous pages, conservation laws are imposed to determine the contact terms that participate in the EFT, depicted in figure 7. In the present work, we will only consider the $\Omega^- N \to \Omega^- N$ channel.

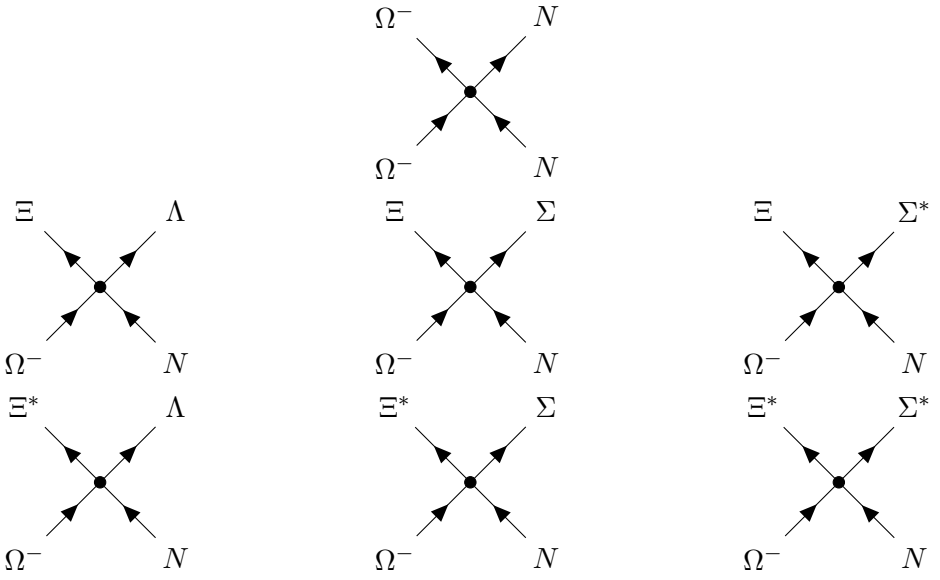

Figure 7: Contact diagrams to consider in the interaction.

The charge of the outgoing baryons should be taken in accordance to the incoming nucleon, in the same way as they appeared in the one meson exchange case. The angular momenta and isospins are also completely analogous.

2.2 $N\Omega$ vertices

Having studied the leading order diagrams contributing to the $N\Omega$ interaction, we compute the vertices using the Lagrangian corresponding to each case. The ultimate goal is to compute the $\mathrm{p}\Omega \to \mathrm{p}\Omega$ leading order potential. Therefore, we will need to study the $\mathrm{p}\eta\bar{\mathrm{p}}$ and $\Omega\eta\bar{\Omega}$ couplings.

2.2.1 $\mathrm{p}\eta\bar{\mathrm{p}}$ coupling

The Lagrangian describing the strong interaction in the octet is given by [OR97, Pic95]

$$\mathcal{L}_{\mathrm{O}} = \mathrm{tr}[\bar{B}(\mathrm{i}\gamma^\mu \nabla_\mu - m_B)B] + D\,\mathrm{tr}[\bar{B}\gamma^\mu\gamma_5\{u_\mu, B\}] + F\,\mathrm{tr}[\bar{B}\gamma^\mu\gamma_5[u_\mu, B]], \tag{2.1}$$

where m_B is the baryon mass and D and F are low energy constants. We can expand the covariant derivative as $\nabla_\mu B = \partial_\mu B + [\Gamma_\mu, B]$, which leaves

$$\mathcal{L}_{\mathrm{O}} = \mathrm{i}\,\mathrm{tr}[\bar{B}\gamma^\mu\partial_\mu B] + \mathrm{i}\,\mathrm{tr}[\bar{B}\gamma^\mu[\Gamma_\mu, B]] - m_B\,\mathrm{tr}[\bar{B}B] + D\gamma^\mu\gamma_5\,\mathrm{tr}[\bar{B}\{u_\mu, B\}] + F\gamma^\mu\gamma_5\,\mathrm{tr}[\bar{B}[u_\mu, B]]. \tag{2.2}$$

In the last two expressions, we have vector and axial vector currents

$$\begin{aligned} \Gamma_\mu &= (u\partial_\mu u^\dagger + u^\dagger\partial_\mu u)/2, \\ u_\mu &= \mathrm{i}(u\partial_\mu u^\dagger - u^\dagger\partial_\mu u)/2, \end{aligned} \tag{2.3}$$

with the u operator defined by $u^2 = \exp(\mathrm{i}\sqrt{2}\phi/f)$ and f the meson decay constant. In the one meson exchange model, we can expand u up to first order in ϕ, as

$$u \simeq 1 + \frac{\mathrm{i}}{\sqrt{2}f}\phi, \tag{2.4}$$

which lets us rewrite the currents as

$$\begin{aligned}\Gamma_\mu &= 0,\\ u_\mu &= \frac{1}{\sqrt{2}f}\partial_\mu\phi.\end{aligned} \tag{2.5}$$

This allows us to turn the Lagrangian into

$$\mathcal{L}_{\mathrm{O}} = \mathrm{i}\,\mathrm{tr}[\bar{B}\gamma^\mu\partial_\mu B] - m_B\,\mathrm{tr}[\bar{B}B] + \frac{D}{\sqrt{2}f}\,\mathrm{tr}[\bar{B}\gamma^\mu\gamma_5\{\partial_\mu\phi, B\}] + \frac{F}{\sqrt{2}f}\,\mathrm{tr}[\bar{B}\gamma^\mu\gamma_5[\partial_\mu\phi, B]]. \tag{2.6}$$

The ground-state octet baryon and meson matrices are

$$\begin{aligned}
B &= \begin{pmatrix} \frac{1}{\sqrt{2}}\Sigma^0 + \frac{1}{\sqrt{6}}\Lambda & \Sigma^+ & \mathrm{p} \\ \Sigma^- & -\frac{1}{\sqrt{2}}\Sigma^0 + \frac{1}{\sqrt{6}}\Lambda & \mathrm{n} \\ \Xi^- & \Xi^0 & -\frac{2}{\sqrt{6}}\Lambda \end{pmatrix},\\
\bar{B} &= \begin{pmatrix} \frac{1}{\sqrt{2}}\overline{\Sigma^0} + \frac{1}{\sqrt{6}}\bar{\Lambda} & \overline{\Sigma^-} & \overline{\Xi^-} \\ \overline{\Sigma^+} & -\frac{1}{\sqrt{2}}\overline{\Sigma^0} + \frac{1}{\sqrt{6}}\bar{\Lambda} & \overline{\Xi^0} \\ \bar{\mathrm{p}} & \bar{\mathrm{n}} & -\frac{2}{\sqrt{6}}\bar{\Lambda} \end{pmatrix},\\
\phi &= \begin{pmatrix} \frac{1}{\sqrt{2}}\pi^0 + \frac{1}{\sqrt{6}}\eta & \pi^+ & \mathrm{K}^+ \\ \pi^- & -\frac{1}{\sqrt{2}}\pi^0 + \frac{1}{\sqrt{6}}\eta & \mathrm{K}^0 \\ \mathrm{K}^- & \overline{\mathrm{K}^0} & -\frac{2}{\sqrt{6}}\eta \end{pmatrix}.
\end{aligned} \tag{2.7}$$

The first example we will look at is the $\mathrm{p}\eta\bar{\mathrm{p}}$ vertex, which appears in the first of the proton diagrams. For this term, we get

$$\begin{aligned}
B &= \begin{pmatrix} 0 & 0 & \mathrm{p} \\ 0 & 0 & 0 \\ 0 & 0 & 0 \end{pmatrix},\\
\bar{B} &= \begin{pmatrix} 0 & 0 & 0 \\ 0 & 0 & 0 \\ \bar{\mathrm{p}} & 0 & 0 \end{pmatrix},\\
\phi &= \frac{1}{\sqrt{6}}\begin{pmatrix} \eta & 0 & 0 \\ 0 & \eta & 0 \\ 0 & 0 & -2\eta \end{pmatrix}.
\end{aligned} \tag{2.8}$$

The first term in the Lagrangian, the kinetic term, can be calculated as follows,

$$\begin{aligned}
\mathrm{i}\,\mathrm{tr}[\bar{B}\gamma^\mu\partial_\mu B] &= \mathrm{i}\,\mathrm{tr}\left[\begin{pmatrix} 0 & 0 & 0 \\ 0 & 0 & 0 \\ \bar{\mathrm{p}} & 0 & 0 \end{pmatrix}\gamma^\mu\begin{pmatrix} 0 & 0 & \partial_\mu\mathrm{p} \\ 0 & 0 & 0 \\ 0 & 0 & 0 \end{pmatrix}\right]\\
&= \mathrm{i}\gamma^\mu\,\mathrm{tr}\begin{pmatrix} 0 & 0 & 0 \\ 0 & 0 & 0 \\ 0 & 0 & \bar{\mathrm{p}}\gamma^\mu\partial_\mu\mathrm{p} \end{pmatrix}\\
&= \mathrm{i}\bar{\mathrm{p}}\gamma^\mu\partial_\mu\mathrm{p}.
\end{aligned} \tag{2.9}$$

The computation of the mass term is nearly identical,

$$\begin{aligned}
-M_B\,\mathrm{tr}[\bar{B}B] &= -M_B\,\mathrm{tr}\left[\begin{pmatrix} 0 & 0 & 0 \\ 0 & 0 & 0 \\ \bar{\mathrm{p}} & 0 & 0 \end{pmatrix}\begin{pmatrix} 0 & 0 & \mathrm{p} \\ 0 & 0 & 0 \\ 0 & 0 & 0 \end{pmatrix}\right]\\
&= -M_B\,\mathrm{tr}\begin{pmatrix} 0 & 0 & 0 \\ 0 & 0 & 0 \\ 0 & 0 & \bar{\mathrm{p}}\mathrm{p} \end{pmatrix}\\
&= -M_B\bar{\mathrm{p}}\mathrm{p}.
\end{aligned} \tag{2.10}$$

As for the rest of the terms, we need the commutator and the anticommutator of $\partial_\mu\phi$ and B. Hence, we need the products

$$\begin{aligned}(\partial_\mu\phi)B &= \frac{1}{\sqrt{6}}\begin{pmatrix}\partial_\mu\eta & 0 & 0\\ 0 & \partial_\mu\eta & 0\\ 0 & 0 & -2\partial_\mu\eta\end{pmatrix}\begin{pmatrix}0 & 0 & \mathrm{p}\\ 0 & 0 & 0\\ 0 & 0 & 0\end{pmatrix}\\ &= \frac{1}{\sqrt{6}}\begin{pmatrix}0 & 0 & (\partial_\mu\eta)\mathrm{p}\\ 0 & 0 & 0\\ 0 & 0 & 0\end{pmatrix},\\ B\partial_\mu\phi &= \frac{1}{\sqrt{6}}\begin{pmatrix}0 & 0 & \mathrm{p}\\ 0 & 0 & 0\\ 0 & 0 & 0\end{pmatrix}\begin{pmatrix}\partial_\mu\eta & 0 & 0\\ 0 & \partial_\mu\eta & 0\\ 0 & 0 & -2\partial_\mu\eta\end{pmatrix}\\ &= \frac{1}{\sqrt{6}}\begin{pmatrix}0 & 0 & -2(\partial_\mu\eta)\mathrm{p}\\ 0 & 0 & 0\\ 0 & 0 & 0\end{pmatrix}.\end{aligned} \tag{2.11}$$

From here, we get the last two terms: the one coupled by D,

$$\begin{aligned}\frac{D}{\sqrt{2}f}\,\mathrm{tr}[\bar{B}\gamma^\mu\gamma_5\{\partial_\mu\phi, B\}] &= \frac{-D}{\sqrt{3}f}\,\mathrm{tr}\left[\begin{pmatrix}0 & 0 & 0\\ 0 & 0 & 0\\ \bar{\mathrm{p}} & 0 & 0\end{pmatrix}\gamma^\mu\gamma_5\begin{pmatrix}0 & 0 & (\partial_\mu\eta)\mathrm{p}\\ 0 & 0 & 0\\ 0 & 0 & 0\end{pmatrix}\right]\\ &= \frac{-D}{2\sqrt{3}f}\,\mathrm{tr}\begin{pmatrix}0 & 0 & 0\\ 0 & 0 & 0\\ 0 & 0 & \bar{\mathrm{p}}\gamma^\mu\gamma_5(\partial_\mu\eta)\mathrm{p}\end{pmatrix}\\ &= \frac{-D}{2\sqrt{3}f}\bar{\mathrm{p}}\gamma^\mu\gamma_5(\partial_\mu\eta)\mathrm{p},\end{aligned} \tag{2.12}$$

and the one coupled by F,

$$\begin{aligned}\frac{F}{\sqrt{2}f}\,\mathrm{tr}[\bar{B}\gamma^\mu\gamma_5[\partial_\mu\phi, B]] &= \frac{\sqrt{3}F}{2f}\,\mathrm{tr}\left[\begin{pmatrix}0 & 0 & 0\\ 0 & 0 & 0\\ \bar{\mathrm{p}} & 0 & 0\end{pmatrix}\gamma^\mu\gamma_5\begin{pmatrix}0 & 0 & (\partial_\mu\eta)\mathrm{p}\\ 0 & 0 & 0\\ 0 & 0 & 0\end{pmatrix}\right]\\ &= \frac{\sqrt{3}F}{2f}\,\mathrm{tr}\begin{pmatrix}0 & 0 & 0\\ 0 & 0 & 0\\ 0 & 0 & \bar{\mathrm{p}}\gamma^\mu\gamma_5(\partial_\mu\eta)\mathrm{p}\end{pmatrix}\\ &= \frac{\sqrt{3}F}{2f}\bar{\mathrm{p}}\gamma^\mu\gamma_5(\partial_\mu\eta)\mathrm{p}.\end{aligned} \tag{2.13}$$

Adding all of the terms, we get the Lagrangian for this vertex,

$$\mathcal{L}_{\mathrm{p}\eta\bar{\mathrm{p}}} = \mathrm{i}\bar{\mathrm{p}}\gamma^\mu(\partial_\mu)\mathrm{p} - m_{\mathrm{p}}\bar{\mathrm{p}}\mathrm{p} + \frac{3F-D}{2\sqrt{3}f}\bar{\mathrm{p}}\gamma^\mu\gamma_5(\partial_\mu\eta)\mathrm{p}. \tag{2.14}$$

The contribution to the potential is this same Lagrangian stripped of fields, introducing the particles involved in the vertex in spinorial form. However, the kinetic and mass terms can be ignored, since the η exchange does not appear, so

$$\begin{aligned}\mathcal{L}_{\mathrm{p}\eta\bar{\mathrm{p}}} &\simeq \frac{3F-D}{2\sqrt{3}f}\bar{\mathrm{p}}\gamma^\mu\gamma_5(\partial_\mu\eta)\mathrm{p}\\ &\equiv C_{\mathrm{p}\eta\bar{\mathrm{p}}}\bar{\mathrm{p}}\gamma^\mu\gamma_5(\partial_\mu\eta)\mathrm{p},\end{aligned} \tag{2.15}$$

from where the contribution is

$$\Gamma_{\mathrm{p}\eta\bar{\mathrm{p}}} = C_{\mathrm{p}\eta\bar{\mathrm{p}}}\bar{u}(p_1')\gamma^\mu\gamma_5 q_\mu u(p_1), \tag{2.16}$$

with Dirac spinors given by

$$u(p) = \sqrt{\frac{E+m_{\mathrm{p}}}{2E}} \begin{pmatrix} \chi \\ \frac{\vec{\sigma}\cdot\vec{p}}{E+m_{\mathrm{p}}}\chi \end{pmatrix}. \tag{2.17}$$

As for the coupling constant, we use the values given by [Spr99, BSS93, JOR02],

$$\begin{aligned} F &= 0.50, \\ D &= 0.80, \\ f &= 93.0\,\mathrm{MeV}. \end{aligned} \tag{2.18}$$

These values yield the constant for the vertex,

$$\begin{aligned} C_{\mathrm{p}\eta\bar{\mathrm{p}}} &= \frac{3F-D}{2\sqrt{3}f} \\ &\approx 2.17\cdot 10^{-3}\,\mathrm{MeV}^{-1}. \end{aligned} \tag{2.19}$$

We evaluate the time and space terms in the Γ operator separately. Beginning by the time component, we have

$$\begin{aligned} \bar{u}(p_1')\gamma^0\gamma_5 q_0 u(p_1) &= \sqrt{\frac{(E'+m_{\mathrm{p}})(E+m_{\mathrm{p}})}{4E'E}} \begin{pmatrix} \chi^\dagger & -\frac{\vec{\sigma}\cdot\vec{k}'}{E'+m_{\mathrm{p}}}\chi^\dagger \end{pmatrix} \gamma^0\gamma_5 \begin{pmatrix} \chi \\ \frac{\vec{\sigma}\cdot\vec{k}}{E+m_{\mathrm{p}}}\chi \end{pmatrix} q_0 \\ &= \sqrt{\frac{(E'+m_{\mathrm{p}})(E+m_{\mathrm{p}})}{4E'E}} \begin{pmatrix} \chi^\dagger & -\frac{\vec{\sigma}\cdot\vec{k}'}{E'+m_{\mathrm{p}}}\chi^\dagger \end{pmatrix} \gamma^0 \begin{pmatrix} \frac{\vec{\sigma}\cdot\vec{k}}{E+m_{\mathrm{p}}}\chi \\ \chi \end{pmatrix} q_0 \\ &= \sqrt{\frac{(E'+m_{\mathrm{p}})(E+m_{\mathrm{p}})}{4E'E}} \begin{pmatrix} \chi^\dagger & -\frac{\vec{\sigma}\cdot\vec{k}'}{E'+m_{\mathrm{p}}}\chi^\dagger \end{pmatrix} \begin{pmatrix} \frac{\vec{\sigma}\cdot\vec{k}}{E+m_{\mathrm{p}}}\chi \\ -\chi \end{pmatrix} q_0 \\ &= \sqrt{\frac{(E'+m_{\mathrm{p}})(E+m_{\mathrm{p}})}{4E'E}}\vec{\sigma}\cdot\left(\frac{\vec{k}}{E+m_{\mathrm{p}}}+\frac{\vec{k}'}{E'+m_{\mathrm{p}}}\right) q_0. \end{aligned} \tag{2.20}$$

Considering energy conservation, we get $E = E'$, and in the non-relativistic limit we have $E \simeq m_{\mathrm{p}}$, so

$$\bar{u}(p_1')\gamma^0\gamma_5 q_0 u(p_1) = \frac{\vec{\sigma}\cdot(\vec{k}+\vec{k}')q_0}{2m_{\mathrm{p}}}. \tag{2.21}$$

The calculation for the space components is similar, but one has to consider the changed sign due to the metric. Therefore, we have

$$\begin{aligned} \bar{u}(p_1')\gamma^j\gamma_5 q_j u(p_1) &= \sqrt{\frac{(E'+m_{\mathrm{p}})(E+m_{\mathrm{p}})}{4E'E}} \begin{pmatrix} \chi^\dagger & -\frac{\vec{\sigma}\cdot\vec{k}'}{E'+m_{\mathrm{p}}}\chi^\dagger \end{pmatrix} \gamma^j\gamma_5 \begin{pmatrix} \chi \\ \frac{\vec{\sigma}\cdot\vec{k}}{E+m_{\mathrm{p}}}\chi \end{pmatrix} q_j \\ &= \sqrt{\frac{(E'+m_{\mathrm{p}})(E+m_{\mathrm{p}})}{4E'E}} \begin{pmatrix} \chi^\dagger & -\frac{\vec{\sigma}\cdot\vec{k}'}{E'+m_{\mathrm{p}}}\chi^\dagger \end{pmatrix} \gamma^j \begin{pmatrix} \frac{\vec{\sigma}\cdot\vec{k}}{E+m_{\mathrm{p}}}\chi \\ \chi \end{pmatrix} q_j \\ &= \sqrt{\frac{(E'+m_{\mathrm{p}})(E+m_{\mathrm{p}})}{4E'E}} \begin{pmatrix} \chi^\dagger & -\frac{\vec{\sigma}\cdot\vec{k}'}{E'+m_{\mathrm{p}}}\chi^\dagger \end{pmatrix} \begin{pmatrix} \hat{\sigma}^j\chi \\ -\hat{\sigma}^j\frac{\vec{\sigma}\cdot\vec{k}}{E+m_{\mathrm{p}}}\chi \end{pmatrix} q_j \\ &= \sqrt{\frac{(E'+m_{\mathrm{p}})(E+m_{\mathrm{p}})}{4E'E}} \left(\vec{\sigma} + \frac{\vec{\sigma}\cdot\vec{k}'}{E'+m_{\mathrm{p}}}\vec{\sigma}\frac{\vec{\sigma}\cdot\vec{k}}{E+m_{\mathrm{p}}}\right)\cdot\vec{q}. \end{aligned} \tag{2.22}$$

Again, we apply energy conservation and the non-relativistic limit, and can approximate

$$\bar{u}(p_1')\gamma^j\gamma_5 q_j u(p_1) \simeq -\vec{\sigma}\cdot\vec{q}. \tag{2.23}$$

We may, now, add both terms and get the result for the vertex operator,

$$\Gamma_{\mathrm{p}\eta\bar{\mathrm{p}}} = C_{\mathrm{p}\eta\bar{\mathrm{p}}}\left[\frac{\vec{\sigma}\cdot(\vec{k}+\vec{k}')q_0}{2m_{\mathrm{p}}} - \vec{\sigma}\cdot\vec{q}\right]. \tag{2.24}$$

2.2.2 $\Omega\eta\bar{\Omega}$ coupling

As for the decuplet coupling, we will use the strong decuplet-decuplet components of the heavy baryon chiral perturbation theory Lagrangian [JM91], that is

$$\mathcal{L}_{\mathrm{D}} = -\mathrm{i}\bar{T}^{\mu}(v\cdot\nabla)T_{\mu} + \Delta m\bar{T}^{\mu}T_{\mu} + 2\mathcal{H}\bar{T}^{\mu}\hat{\mathbb{S}}_{\nu}u^{\nu}T_{\mu}, \tag{2.25}$$

where $\vec{\mathbb{S}}$ is the octet spin operator, v is a velocity vector relating the baryon fields, Δm is the baryon-octet mass difference, $\mathcal{H}$ is a low energy constant, and T is the totally symmetric three-index tensor representing the decuplet baryons, which has components given by

$$\begin{aligned}
&T^{111} = \Delta^{++}, \qquad T^{112} = \frac{1}{\sqrt{3}}\Delta^{+}, \quad T^{113} = \frac{1}{\sqrt{3}}\Sigma^{*+},\\
&T^{122} = \frac{1}{\sqrt{3}}\Delta^{0}, \quad T^{123} = \frac{1}{\sqrt{6}}\Sigma^{*0},\\
&T^{133} = \frac{1}{\sqrt{3}}\Xi^{*0},\\
&T^{222} = \Delta^{-}, \qquad T^{223} = \frac{1}{\sqrt{3}}\Sigma^{*-},\\
&T^{233} = \frac{1}{\sqrt{3}}\Xi^{*-},\\
&T^{333} = \Omega^{-}.
\end{aligned} \tag{2.26}$$

From here, we compute its contractions with the meson field to obtain the third term in the last Lagrangian, for we neglect the rest mass and kinetic terms.

Now, for the $\Omega\eta\bar{\Omega}$ vertex, we have baryons

$$\begin{aligned}
T^{dab} &= T^{333}\\
&= \Omega,\\
T^{abc} &= \bar{T}_{333}\\
&= \bar{\Omega},
\end{aligned} \tag{2.27}$$

and meson field

$$\begin{aligned}
\phi^{c}_{d} &= \phi^{3}_{3}\\
&= \frac{-1}{\sqrt{3}f}\eta.
\end{aligned} \tag{2.28}$$

For the vertex calculation, again, we can ignore both the mass and kinetic terms, so we have Lagrangian

$$\begin{aligned}
\mathcal{L}_{\Omega\eta\bar{\Omega}} &\simeq -\frac{2\mathcal{H}}{\sqrt{3}f}\bar{\Omega}\mathbb{S}^{\mu}(\partial_{\mu}\eta)\Omega\\
&\equiv C_{\Omega\eta\bar{\Omega}}\bar{\Omega}\mathbb{S}^{\mu}(\partial_{\mu}\eta)\Omega,
\end{aligned} \tag{2.29}$$

from where the contribution is

$$\begin{aligned}
\Gamma_{\bar{\Omega}\eta\Omega} &= -C_{\Omega\eta\bar{\Omega}}\hat{\mathbb{S}}^{\mu}q_{\mu}\\
&= -C_{\Omega\eta\bar{\Omega}}(\hat{\mathbb{S}}^{0}q_{0} - \vec{\mathbb{S}}\cdot\vec{q}).
\end{aligned} \tag{2.30}$$

Again, we compute the coupling constant using the values given in [Spr99, BSS93, JOR02], in particular $\mathcal{H} = -1.90$, and get

$$\begin{aligned}
C_{\Omega\eta\bar{\Omega}} &= -\frac{2}{\sqrt{3}}\frac{\mathcal{H}}{f}\\
&\approx 2.36\cdot 10^{-2}\ \mathrm{MeV}^{-1}.
\end{aligned} \tag{2.31}$$

2.3 Leading order $\mathrm{p}\Omega \to \mathrm{p}\Omega$ potential derivation

By studying the diagrams and their orders, we have seen that, at LO, we only need to include for the elastic $\mathrm{p}\Omega$ interaction a contact term and an η exchange term. This means that we can write

$$\hat{V}_{\mathrm{p}\Omega} = \hat{V}_{\mathrm{ct}} + \hat{V}_{\eta}. \tag{2.32}$$

We will study both terms in order to evaluate the potential matrix elements.

Since we are going to evaluate multiple spin operators, we should explain the notation for them. We write $\vec{\mathbb{S}}$ for the Ω particle spin, $\vec{\sigma}/2$ for the proton spin, $\vec{S} = \vec{\mathbb{S}} + \vec{\sigma}/2$ for the total spin, $\vec{L}$ for the relative angular momentum and $\vec{J} = \vec{L} + \vec{S}$ for the total angular momentum.

2.3.1 Contact potential

While combining spin, isospin and momentum while respecting the symmetries of the system, keeping to leading order we can only have a central and a spin-spin term in the contact potential. Therefore, we may write

$$\hat{V}_{\mathrm{ct}}(q) = C_0^0 + C_0^1 \vec{\mathbb{S}} \cdot \vec{\sigma}, \tag{2.33}$$

where C_0^0 and C_0^1 are low energy constants. Notice that we have not included any form factor in it, so the only free parameters we have as of now are C_0^0 and C_0^1. To get this potential into the position representation, we need to perform a Fourier transformation on it. This produces a Dirac delta function, which we will regularize by replacing it for a smeared function f_δ,

$$\hat{V}_{\mathrm{ct}}(\vec{r}) = \left(C_0^0 + C_0^1 \vec{\mathbb{S}} \cdot \vec{\sigma}\right) f_\delta(r), \tag{2.34}$$

which we choose to be a Gaussian,

$$f_\delta(r) = \frac{e^{-(r/\delta)^2}}{\pi^{3/2}\delta^3}. \tag{2.35}$$

Usually, the value of the δ parameter is taken such that it represents the energy scale of the first heavy meson excluded at LO; in this case, the ω meson. We may use, for example, $\delta = \sqrt{2}/m_\omega$.

To find these matrix elements, one has to compute the $\vec{\mathbb{S}} \cdot \vec{\sigma}$ matrix elements. To do so, we compute the scalar product in terms of the total spin, as usual,

$$\begin{aligned} \vec{\mathbb{S}} \cdot \vec{\sigma} &= 2\vec{\mathbb{S}} \cdot \frac{\vec{\sigma}}{2} \\ &= \hat{S}^2 - \hat{\mathbb{S}}^2 - \frac{\hat{\sigma}^2}{4} \\ &= \hat{S}^2 - \frac{9}{2}, \end{aligned} \tag{2.36}$$

using both of the particles' spins. Hence, the matrix elements are

$$\langle (1/2,3/2) S' M_S' | \, \vec{\mathbb{S}} \cdot \vec{\sigma} \, | (1/2,3/2) S M_S \rangle = \left[S(S+1) - \frac{9}{2} \right] \delta_{SS'} \delta_{M_S M_S'}. \tag{2.37}$$

2.3.2 η exchange potential

Given that we have already computed the vertices for the η exchange diagram, we will build the η exchange potential connecting both of the Γ operators with the meson propagator, so

$$\begin{aligned} \hat{V}_\eta(q) &= \mathrm{i}\Gamma_{\mathrm{p}\eta\bar{\mathrm{p}}} \frac{\mathrm{i}}{q^2 - {m_\eta}^2} \Gamma_{\Omega\eta\bar{\Omega}} \\ &= C_{\mathrm{p}\eta\bar{\mathrm{p}}} \left[\frac{\vec{\sigma} \cdot (\vec{k} + \vec{k}') q_0}{2M_{\mathrm{p}}} - \vec{\sigma} \cdot \vec{q} \right] C_{\Omega\eta\bar{\Omega}} \frac{\hat{\mathbb{S}}^0 q_0 - \vec{\mathbb{S}} \cdot \vec{q}}{q^2 - {m_\eta}^2}. \end{aligned} \tag{2.38}$$

Here, we take the static approximation and get $q_0 \approx 0$, so the potential becomes

$$\hat{V}_\eta(\vec{q}) = -C_{\mathrm{p}\eta\bar{\mathrm{p}}} C_{\Omega\eta\bar{\Omega}} \frac{(\vec{\mathbb{S}}\cdot\vec{q})(\vec{\sigma}\cdot\vec{q})}{\vec{q}^{\,2} + {m_\eta}^2}. \tag{2.39}$$

This gives the potential in momentum space. To get it in coordinate space we only need to perform a Fourier transform,

$$\begin{aligned}
\hat{V}_\eta(\vec{r}) &= -C_{\mathrm{p}\eta\bar{\mathrm{p}}} C_{\Omega\eta\bar{\Omega}} \int_{\mathbb{R}^3} \frac{\mathrm{d}\vec{q}}{(2\pi)^3} e^{\mathrm{i}\vec{q}\cdot\vec{r}} \frac{(\vec{\mathbb{S}}\cdot\vec{q})(\vec{\sigma}\cdot\vec{q})}{\vec{q}^{\,2} + {m_\eta}^2} \\
&= C_{\mathrm{p}\eta\bar{\mathrm{p}}} C_{\Omega\eta\bar{\Omega}} \hat{\mathbb{S}}^i \hat{\sigma}^j \partial_i \partial_j \int_{\mathbb{R}^3} \frac{\mathrm{d}\vec{q}}{(2\pi)^3} \frac{e^{\mathrm{i}\vec{q}\cdot\vec{r}}}{\vec{q}^{\,2} + {m_\eta}^2} \\
&= C_{\mathrm{p}\eta\bar{\mathrm{p}}} C_{\Omega\eta\bar{\Omega}} \hat{\mathbb{S}}^i \hat{\sigma}^j \partial_i \partial_j \frac{e^{-m_\eta r}}{4\pi r}.
\end{aligned} \tag{2.40}$$

The jump between the first and second lines is easy to miss: since we have the product $\mathrm{i}\vec{q}\cdot\vec{r}$ in an exponent, differentiating with respect to x_i will make an $\mathrm{i}q_i$ factor drop down, so the two scalar products in the first line may be replaced by the partial derivatives in the second line. The last integral was a known Fourier transform: the well-known Yukawa potential. Now, using the properties of consecutive derivation, the potential becomes

$$V_\eta(\vec{r}) = C_{\mathrm{p}\eta\bar{\mathrm{p}}} C_{\Omega\eta\bar{\Omega}} \left[\vec{\mathbb{S}}\cdot\vec{\sigma} \frac{1}{r}\frac{\mathrm{d}}{\mathrm{d}r} + (\vec{\mathbb{S}}\cdot\hat{r})(\vec{\sigma}\cdot\hat{r}) \left(\frac{\mathrm{d}^2}{\mathrm{d}r^2} - \frac{1}{r}\frac{\mathrm{d}}{\mathrm{d}r} \right) \right] \frac{e^{-m_\eta r}}{4\pi r}. \tag{2.41}$$

Here, we start to notice that we will be left with two terms, each with an operator multiplied by a radial function. The radial functions will be easily obtained by differentiating the right-side function repeatedly. To save work, however, we should study the second operator first. We may rewrite it as

$$\begin{aligned}
(\vec{\mathbb{S}}\cdot\hat{r})(\vec{\sigma}\cdot\hat{r}) &= \sum_{\mu,\mu'} (-1)^\mu \hat{\mathbb{S}}_\mu \hat{r}_{-\mu} (-1)^{-\mu'} \hat{\sigma}_{-\mu'} \hat{r}_{\mu'} \\
&= \frac{4\pi}{3} \sum_{L,M_L} (-1)^{M_L} \left[\vec{\mathbb{S}} \times \vec{\sigma} \right]^L_{-M_L} \cdot \left[\vec{Y}_1 \times \vec{Y}_1 \right]^L_{M_L} \\
&= \frac{1}{3}\vec{\mathbb{S}}\cdot\vec{\sigma} + \sum_{M_L} (-1)^{M_L} \left[\vec{\mathbb{S}} \times \vec{\sigma} \right]^2_{-M_L} \cdot [\hat{r} \times \hat{r}]^2_{M_L},
\end{aligned} \tag{2.42}$$

having used $\hat{r} = \sqrt{\frac{4\pi}{3}}\vec{Y}_1$ and developed

$$\begin{aligned}
\hat{r}_{-\mu}\hat{r}_{\mu'} &= \frac{4\pi}{3} Y_{1-\mu} Y_{1\mu'} \\
&= \frac{4\pi}{3} \sum_{L,M_L} \langle L M_L | 1-\mu 1\mu' \rangle \left[\vec{Y}_1 \times \vec{Y}_1 \right]^L_{M_L}.
\end{aligned} \tag{2.43}$$

By defining $\hat{O}_{\mathrm{T}}/3$ as the larger sum operator in the final expression, we may rewrite the interaction as

$$\begin{aligned}
\hat{V}_\eta(\vec{r}) &= C_{\mathrm{p}\eta\bar{\mathrm{p}}} C_{\Omega\eta\bar{\Omega}} \left[\vec{\mathbb{S}}\cdot\vec{\sigma} \frac{1}{r}\frac{\mathrm{d}}{\mathrm{d}r} + \frac{1}{3}(\vec{\mathbb{S}}\cdot\vec{\sigma} + \hat{O}_{\mathrm{T}}) \left(\frac{\mathrm{d}^2}{\mathrm{d}r^2} - \frac{1}{r}\frac{\mathrm{d}}{\mathrm{d}r} \right) \right] \frac{e^{-m_\eta r}}{4\pi r} \\
&= \frac{C_{\mathrm{p}\eta\bar{\mathrm{p}}} C_{\Omega\eta\bar{\Omega}}}{3} \left[\vec{\mathbb{S}}\cdot\vec{\sigma}\nabla^2 + \hat{O}_{\mathrm{T}} \left(\frac{\mathrm{d}^2}{\mathrm{d}r^2} - \frac{1}{r}\frac{\mathrm{d}}{\mathrm{d}r} \right) \right] \frac{e^{-m_\eta r}}{4\pi r}.
\end{aligned} \tag{2.44}$$

The last task left in order to obtain the form of the potential is to compute the radial functions, for which we only need the first two derivatives and the Laplacian of the right-side function, which we label f. The first two derivatives are straightforward,

$$\begin{aligned}
\frac{\mathrm{d}f}{\mathrm{d}r} &= -\left(m_\eta + \frac{1}{r} \right) \frac{e^{-m_\eta r}}{4\pi r}, \\
\frac{\mathrm{d}^2 f}{\mathrm{d}r^2} &= \left({m_\eta}^2 + \frac{2m_\eta}{r} + \frac{2}{r^2} \right) \frac{e^{-m_\eta r}}{4\pi r}.
\end{aligned} \tag{2.45}$$

The Laplacian is a bit longer to compute. We start by calculating it explicitly and get it broken up in three terms,

$$\begin{aligned}\nabla^2(e^{-m_\eta r}/r) &= \vec{\nabla}\cdot\vec{\nabla}(e^{-m_\eta r}/r)\\ &= \vec{\nabla}\cdot\left[\vec{\nabla}(1/r)e^{-m_\eta r} + \frac{1}{r}\vec{\nabla}(e^{-m_\eta r})\right]\\ &= \nabla^2(1/r)e^{-m_\eta r} + 2\vec{\nabla}(1/r)\cdot\vec{\nabla}(e^{-m_\eta r}) + \frac{1}{r}\nabla^2(e^{-m_\eta r}).\end{aligned} \tag{2.46}$$

The first term is going to be the tricky one. Either way, we need to calculate two gradients, which we will do in spherical coordinates,

$$\begin{aligned}\vec{\nabla}(1/r) &= \partial_r(1/r)\hat{r}\\ &= -\frac{\vec{r}}{r^3},\\ \vec{\nabla}(e^{-m_\eta r}) &= \partial_r(e^{-m_\eta r})\hat{r}\\ &= -m_\eta e^{-m_\eta r}\frac{\vec{r}}{r}.\end{aligned} \tag{2.47}$$

From here, calculating the last two terms is straightforward, using spherical coordinates,

$$\begin{aligned}\vec{\nabla}(1/r)\cdot\vec{\nabla}(e^{-m_\eta r}) &= \left(-\frac{\vec{r}}{r^3}\right)\cdot\left(-m_\eta e^{-m_\eta r}\frac{\vec{r}}{r}\right)\\ &= -\frac{m_\eta e^{-m_\eta r}}{r^2},\end{aligned} \tag{2.48}$$

and

$$\begin{aligned}\nabla^2(e^{-m_\eta r}) &= \vec{\nabla}\cdot\vec{\nabla}(e^{-m_\eta r})\\ &= \frac{1}{r^2}\partial_r[r^2\hat{r}\cdot\vec{\nabla}(e_{-m_\eta r})]\\ &= -\frac{m_\eta}{r^2}\partial_r(r^2e^{-m_\eta r})\\ &= (m_\eta r - 2)\,\frac{m_\eta}{r}e^{-m_\eta r}.\end{aligned} \tag{2.49}$$

However, the first term can not be attacked in a regular way. We actually can compute, for $r \neq 0$,

$$\begin{aligned}\nabla^2(1/r) &= -\vec{\nabla}\cdot(\vec{r}/r^3)\\ &= -\frac{1}{r^2}\partial_r(r^2\hat{r}\cdot\vec{r}/r^3)\\ &= 0,\end{aligned} \tag{2.50}$$

and we can calculate it at the missing point, $r = 0$, by using the divergence theorem for the unit ball $\mathbb{D}^3$, which tells us

$$\begin{aligned}\int_{\mathbb{D}^3}\nabla^2\left(\frac{1}{r}\right)\mathrm{d}V &= \int_{\mathbb{S}^2}\hat{r}\cdot\vec{\nabla}\left(\frac{1}{r}\right)\mathrm{d}S\\ &= -\int_{\mathbb{S}^2}\frac{1}{r^2}\,\mathrm{d}S\\ &= -\int_0^\pi \sin\theta\,\mathrm{d}\theta\int_0^{2\pi}\mathrm{d}\varphi\\ &= -4\pi,\end{aligned} \tag{2.51}$$

and this forces a Dirac delta on the origin, which solves the conundrum,

$$\nabla^2\left(\frac{1}{r}\right) = -4\pi\delta(\vec{r}). \tag{2.52}$$

Joining all of the computations together, we have the Laplacian,

$$\nabla^2 f = {m_\eta}^2 \frac{e^{-m_\eta r}}{4\pi r} - \delta(\vec{r}), \tag{2.53}$$

with which we can write the η exchange potential by writing the radial functions explicitly,

$$\hat{V}_\eta(\vec{r}) = C_{\mathrm{p}\eta\bar{\mathrm{p}}} C_{\Omega\eta\bar{\Omega}} \frac{{m_\eta}^2}{3} \frac{e^{-m_\eta r}}{4\pi r} \left[\vec{\mathbb{S}} \cdot \vec{\sigma} + \left(1 + \frac{3}{m_\eta r} + \frac{3}{(m_\eta r)^2} \right) \hat{O}_{\mathrm{T}} \right]. \tag{2.54}$$

For the first term, we already computed the matrix elements while analyzing the contact potential. Hence, we only need to compute the tensor matrix elements.

2.3.3 Tensor term matrix elements and partial waves

Remember that we defined the $\hat{O}_{\mathrm{T}}$ tensor operator as

$$\langle (L'S')JM_J | \hat{O}_{\mathrm{T}} | (LS)JM_J \rangle = 3 \langle (L'S')JM_J | \sum_\mu (-1)^\mu [\vec{\mathbb{S}} \times \vec{\sigma}]_{-\mu}{}^2 [\hat{r} \times \hat{r}]_\mu{}^2 | (LS)JM_J \rangle . \tag{2.55}$$

In spherical components, we can factor

$$[\hat{r} \times \hat{r}]_\mu{}^2 = \frac{4\pi}{3} \sum_{m,m'} \langle 2\mu | 1m1m' \rangle \, Y_{1m}(\hat{r}) Y_{1m}(\hat{r}). \tag{2.56}$$

This summation of products of spherical harmonics can be rewritten using Clebsch-Gordan coefficients,

$$\sum_{m,m'} \langle LM_L | l_1 m l_2 m' \rangle \, Y_{l_1 m}(\hat{r}) Y_{l_2 m'}(\hat{r}) = \sqrt{\frac{(2l_1+1)(2l_2+1)}{4(2L+1)\pi}} \langle L0 | l_1 0 l_2 0 \rangle \, Y_{LM}(\hat{r}), \tag{2.57}$$

which, particularized to the case with $L = 2$, $M_L = \mu$ and $l_1 = l_2 = 1$, reads

$$\sum_{m,m'} \langle 2\mu | 1m1m' \rangle \, Y_{1m}(\hat{r}) Y_{1m'}(\hat{r}) = \sqrt{\frac{9}{20\pi}} \langle 20 | 1010 \rangle \, Y_{2\mu}(\hat{r}). \tag{2.58}$$

Hence, we get

$$\begin{aligned} [\hat{r} \times \hat{r}]_\mu{}^2 &= \sqrt{\frac{4\pi}{5}} \langle 20 | 1010 \rangle \, Y_{2\mu}(\hat{r}) \\ &= \sqrt{\frac{8\pi}{15}} Y_{2\mu}(\hat{r}). \end{aligned} \tag{2.59}$$

Using this, we have completed the first step for the evaluation of the matrix elements,

$$\langle (L'S')JM_J | \hat{O}_{\mathrm{T}} | (LS)JM_J \rangle = \sqrt{\frac{24\pi}{5}} \langle (L'S')JM_J | \sum_\mu (-1)^\mu [\vec{\mathbb{S}} \times \vec{\sigma}]_{-\mu}{}^2 Y_{2\mu}(\hat{r}) | (LS)JM_J \rangle . \tag{2.60}$$

In the expression, we can identify the coupling of two irreducible rank 2 operators to a rank 0 operator, which lets us rewrite the matrix elements as

$$\langle (L'S')JM_J | \hat{O}_{\mathrm{T}} | (LS)JM_J \rangle = \sqrt{24\pi} \langle (L'S')JM_J | \left[[\vec{\mathbb{S}} \times \vec{\sigma}]^2 \times \vec{Y}_2(\hat{r}) \right]_{00} | (LS)JM_J \rangle . \tag{2.61}$$

This operator is the product of two other operators, characterized by L, M_L and S, M_S, respectively. We should, due to the coupling, express the matrix elements in the coupled representation. That is

$$\begin{aligned} \langle (L'S')JM_J | \hat{O}_{\mathrm{T}} | (LS)JM_J \rangle = & \sqrt{24(2J+1)\pi} \langle JM_J | JM_J 00 \rangle \\ & \begin{Bmatrix} 2 & 2 & 0 \\ L' & S' & J \\ L & S & J \end{Bmatrix} \langle S' || \, [\vec{\mathbb{S}} \times \vec{\sigma}] \, || S \rangle \langle L' || \, \vec{Y}_2 \, || L \rangle . \end{aligned} \tag{2.62}$$

To break the other coupling, one notices that we have two subsystems of spin $3/2$ and $1/2$ coupled to a total spin S with projection M_S. Hence, we have

$$\begin{aligned}\langle (3/2\ 1/2)S'M'_S|\left[\vec{\mathbb{S}}\times\vec{\sigma}\right]_{-\mu}{}^{2}|(3/2\ 1/2)SM_S\rangle =&\sqrt{5(2S+1)}\,\langle S'M'_S|SM_S2\ -\mu\rangle\\ &\begin{Bmatrix}1 & 1 & 2\\ 3/2 & 1/2 & S'\\ 3/2 & 1/2 & S\end{Bmatrix}\langle 3/2||\,\vec{\mathbb{S}}\,||3/2\rangle\,\langle 1/2||\,\vec{\sigma}\,||1/2\rangle\,,\end{aligned} \tag{2.63}$$

whereas the Wigner-Eckart theorem gives

$$\langle S'M'_S|\left[\vec{\mathbb{S}}\times\vec{\sigma}\right]_{-\mu}{}^{2}|SM_S\rangle = \frac{\langle S'M'_S|SM_S2\ -\mu\rangle}{\sqrt{2S'+1}}\,\langle S'||\left[\vec{\mathbb{S}}\times\vec{\sigma}\right]||S\rangle\,. \tag{2.64}$$

Comparison of both terms finally lets us evaluate the desired reduced spin matrix element,

$$\langle S'||\left[\vec{\mathbb{S}}\times\vec{\sigma}\right]||S\rangle = \sqrt{5(2S+1)(2S'+1)}\begin{Bmatrix}1 & 1 & 2\\ 3/2 & 1/2 & S'\\ 3/2 & 1/2 & S\end{Bmatrix}\langle 3/2||\,\vec{\mathbb{S}}\,||3/2\rangle\,\langle 1/2||\,\vec{\sigma}\,||1/2\rangle\,. \tag{2.65}$$

The last matrix elements we need to compute are also possible to calculate by the Wigner-Eckart theorem,

$$\langle L'||\,\vec{Y}_2\,||L\rangle = \sqrt{\frac{5(2L+1)}{4\pi}}\,\langle L'0|L020\rangle\,. \tag{2.66}$$

We can replace all of these terms to get

$$\begin{aligned}\langle (L'S')JM_J|\,\hat{O}_{\mathrm{T}}\,|(LS)JM_J\rangle =&10\sqrt{15(2J+1)(2S+1)(2S'+1)(2L+1)}\\ &\langle L'0|L020\rangle\begin{Bmatrix}2 & 2 & 0\\ L' & S' & J\\ L & S & J\end{Bmatrix}\begin{Bmatrix}1 & 1 & 2\\ 3/2 & 1/2 & S'\\ 3/2 & 1/2 & S\end{Bmatrix}.\end{aligned} \tag{2.67}$$

One relevant particular case is the one with with $L=0$, that is, when the initial system has no relative angular momentum. This implies coupling $J=S$ and $L'=2$. We may also use the properties of the $9j$ symbols and write

$$\begin{aligned}\begin{Bmatrix}2 & 2 & 0\\ L' & S' & J\\ L & S & J\end{Bmatrix} &= \begin{Bmatrix}2 & 2 & 0\\ 2 & S' & S\\ 0 & S & S\end{Bmatrix}\\ &= \begin{Bmatrix}2 & S' & S\\ 0 & S & S\\ 2 & 2 & 0\end{Bmatrix}\\ &= (-1)^{S'+S}\begin{Bmatrix}S' & 2 & S\\ S & 0 & S\\ 2 & 2 & 0\end{Bmatrix}\\ &= \frac{1}{5(2S+1)},\end{aligned} \tag{2.68}$$

which, finally, gets

$$\langle (L'S')JM_J|\,\hat{O}_{\mathrm{T}}\,|(LS)JM_J\rangle = 6\sqrt{15(2S'+1)}\begin{Bmatrix}1 & 1 & 2\\ 3/2 & 1/2 & S'\\ 3/2 & 1/2 & S\end{Bmatrix}. \tag{2.69}$$

Having computed all of the operator matrix elements, we can give a closed expression for the potential matrix elements, both for the contact potential

$$\langle (LS)JM_J|\,\hat{V}_{\rm ct}\,|(LS)JM_J\rangle = \frac{e^{-(r/\delta)^2}}{\pi^{3/2}\delta^3}\left[C_0^0 + C_0^1\left(S(S+1)-\frac{9}{2}\right)\right] \tag{2.70}$$

and for the η exchange potential, sticking to the $L=0$ case,

$$\begin{aligned}\langle (L'S')SM_S|\,\hat{V}_\eta(\vec{r})\,|(0S)SM_S\rangle =& C_{{\rm p}\eta\bar{\rm p}}C_{\Omega\eta\bar{\Omega}}\frac{{m_\eta}^2}{3}\frac{e^{-m_\eta r}}{4\pi r}\left[\left(S(S+1)-\frac{9}{2}\right)\delta_{L',0}\right.\\ &\left.+\left(1+\frac{3}{m_\eta r}+\frac{3}{(m_\eta r)^2}\right)6\sqrt{15(2S'+1)}\begin{Bmatrix}1 & 1 & 2\\ 3/2 & 1/2 & S'\\ 3/2 & 1/2 & S\end{Bmatrix}\delta_{L',2}\right].\end{aligned} \tag{2.71}$$

According to these expressions, the only dependence of the non-zero matrix elements is in the total spins S and S'. We see that the elements with $L'=0$ have the contact and spin-spin potential. Given that $s_{\rm p}=1/2$ and $s_\Omega = 3/2$, said channels are

$$\begin{aligned}{}^3S_1 &\to {}^3S_1,\\ {}^5S_2 &\to {}^5S_2.\end{aligned} \tag{2.72}$$

The other possible couplings, that of the elements with $L'=2$, only get the tensor part of the interaction. Those channels are

$$\begin{aligned}{}^3S_1 &\to {}^3D_1,\\ {}^3S_1 &\to {}^5D_1,\\ {}^5S_2 &\to {}^3D_2,\\ {}^5S_2 &\to {}^5D_2.\end{aligned} \tag{2.73}$$

This way, we only need four $9j$-symbols,

$$\begin{aligned}\begin{Bmatrix}1 & 1 & 2\\ 3/2 & 1/2 & 1\\ 3/2 & 1/2 & 1\end{Bmatrix} &= \frac{-1}{18\sqrt{10}},\\ \begin{Bmatrix}1 & 1 & 2\\ 3/2 & 1/2 & 2\\ 3/2 & 1/2 & 1\end{Bmatrix} &= \frac{-1}{10\sqrt{6}},\\ \begin{Bmatrix}1 & 1 & 2\\ 3/2 & 1/2 & 1\\ 3/2 & 1/2 & 2\end{Bmatrix} &= \frac{1}{10\sqrt{6}},\\ \begin{Bmatrix}1 & 1 & 2\\ 3/2 & 1/2 & 2\\ 3/2 & 1/2 & 2\end{Bmatrix} &= \frac{1}{10}\sqrt{\frac{7}{30}}.\end{aligned} \tag{2.74}$$

2.3.4 σ exchange potential

Up to this point, we have followed the development of the [Flo14] potential. However, a problem we find with said potential is the fact that the η exchange potential is fixed and is repulsive. From [IA+19], however, we expect a net attractive interaction, but this can be achieved if the contact interaction is attractive enough. However, there are evidences [SKH18] that the exchange terms yield an attractive interaction as well.

In [SKH18] it is argued that the σ exchange gives the most attractive part of the meson exchange terms, so we will add said interaction here. Recall that the so called σ meson is the $f_0(500)$ resonance, and is often represented as a correlated pair of pions. We can draw the exchange as follows.

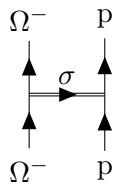

Figure 8: σ exchange diagram.

Unlike the η particle, which is pseudoscalar, the σ meson is a scalar. Therefore, we will find a new potential form without the spin contributions at LO [LS96],

$$\begin{aligned}\hat{V}_\sigma(q) &= \frac{C_{\mathrm{p}\sigma\bar{\mathrm{p}}}C_{\Omega\sigma\bar{\Omega}}}{q^2 - {m_\sigma}^2} \\ &\simeq -\frac{C_{\mathrm{p}\sigma\bar{\mathrm{p}}}C_{\Omega\sigma\bar{\Omega}}}{\vec{q}^{\,2} + {m_\sigma}^2},\end{aligned} \tag{2.75}$$

where in the second line we have taken, again, the static approximation $q_0 \approx 0$. Here we perform the Fourier transform to get to the coordinate space, and obtain the well known Yukawa potential,

$$\begin{aligned}\hat{V}_\sigma(\vec{r}) &= -C_{\mathrm{p}\sigma\bar{\mathrm{p}}}C_{\Omega\sigma\bar{\Omega}}\int\frac{\mathrm{d}\vec{q}}{(2\pi)^3}\frac{e^{\mathrm{i}\vec{q}\cdot\vec{r}}}{\vec{q}^{\,2} + {m_\sigma}^2} \\ &= -C_{\mathrm{p}\sigma\bar{\mathrm{p}}}C_{\Omega\sigma\bar{\Omega}}\frac{e^{-m_\sigma r}}{4\pi r},\end{aligned} \tag{2.76}$$

with no derivative couplings since we are dealing with no Goldstone boson.

As for the $C_{\mathrm{p}\sigma\bar{\mathrm{p}}}$ constant, we may get it from the Walecka-Serot model [SW86]. In [ST20], we find the expression for the NN potential due to σ exchange,

$$V_\sigma^{(NN)}(r) = -\alpha_\sigma\frac{e^{-m_\sigma r}}{r}, \tag{2.77}$$

with $\alpha_\sigma = 6.04$. However, following the σ exchange $N\Omega$ potential we just computed, we obtain another expression for the NN potential, swapping the constant $C_{\Omega\sigma\bar{\Omega}}$ for $C_{\mathrm{p}\sigma\bar{\mathrm{p}}}$,

$$\hat{V}_\sigma^{(NN)}(r) = -{C_{\mathrm{p}\sigma\bar{\mathrm{p}}}}^2\frac{e^{-m_\sigma r}}{4\pi r}, \tag{2.78}$$

since we have the contribution of two $\Gamma_{\mathrm{p}\sigma\bar{\mathrm{p}}}$ vertices. Using this new expression, we can match the two potentials to obtain an expression for the coupling in terms of the α_σ value,

$$\begin{aligned}C_{\mathrm{p}\sigma\bar{\mathrm{p}}} &= \sqrt{4\pi\alpha_\sigma} \\ &\approx 8.71.\end{aligned} \tag{2.79}$$

Since the $C_{\Omega\sigma\bar{\Omega}}$ constant can not be fixed in an analogous way, we will leave it as a free parameter for the model.

2.3.5 Form factor for the exchange potentials

So far, the only regularization we have applied is the cut-off function for the contact interaction used by [Flo14]. We should also, however, add a form factor to each vertex of the exchanged particle potentials to account for the final size of the particles. For it, we choose to use the monopole type form factor

$$F_\Lambda(\vec{q}) = \frac{\Lambda^2}{\Lambda^2 + \vec{q}^{\,2}}. \tag{2.80}$$

To add the form factor to the η exchange potential, it is enough that we write it inside the integral in (2.40) (all steps taken before that are identical). This way, we get

$$\begin{aligned}
\hat{V}_\eta(\vec{r}) &= -C_{\mathrm{p}\eta\bar{\mathrm{p}}}C_{\Omega\eta\bar{\Omega}}\int_{\mathbb{R}^3}\frac{\mathrm{d}\vec{q}}{(2\pi)^3}e^{\mathrm{i}\vec{q}\cdot\vec{r}}\frac{(\vec{\mathbb{S}}\cdot\vec{q})(\vec{\sigma}\cdot\vec{q})}{\vec{q}^{\,2}+{m_\eta}^2}\left(F_{\Lambda_\eta}(q)\right)^2\\
&= -C_{\mathrm{p}\eta\bar{\mathrm{p}}}C_{\Omega\eta\bar{\Omega}}\int_{\mathbb{R}^3}\frac{\mathrm{d}\vec{q}}{(2\pi)^3}e^{\mathrm{i}\vec{q}\cdot\vec{r}}\frac{(\vec{\mathbb{S}}\cdot\vec{q})(\vec{\sigma}\cdot\vec{q})}{\vec{q}^{\,2}+{m_\eta}^2}\left(\frac{{\Lambda_\eta}^2}{{\Lambda_\eta}^2+\vec{q}^{\,2}}\right)^2\\
&= C_{\mathrm{p}\eta\bar{\mathrm{p}}}C_{\Omega\eta\bar{\Omega}}\hat{\mathbb{S}}^i\hat{\sigma}^j\partial_i\partial_j\int_{\mathbb{R}^3}\frac{\mathrm{d}\vec{q}}{(2\pi)^3}\frac{e^{\mathrm{i}\vec{q}\cdot\vec{r}}}{\vec{q}^{\,2}+{m_\eta}^2}\left(\frac{{\Lambda_\eta}^2}{{\Lambda_\eta}^2+\vec{q}^{\,2}}\right)^2\\
&= C_{\mathrm{p}\eta\bar{\mathrm{p}}}C_{\Omega\eta\bar{\Omega}}\hat{\mathbb{S}}^i\hat{\sigma}^j\partial_i\partial_j\int_0^\infty\frac{\mathrm{d}q}{(2\pi)^2}\left(\frac{{\Lambda_\eta}^2}{{\Lambda_\eta}^2+q^2}\right)^2\frac{q^2}{q^2+{m_\eta}^2}\int_{-1}^1\mathrm{d}\cos\theta\, e^{\mathrm{i}qr\cos\theta}\\
&= C_{\mathrm{p}\eta\bar{\mathrm{p}}}C_{\Omega\eta\bar{\Omega}}\hat{\mathbb{S}}^i\hat{\sigma}^j\partial_i\partial_j\left[\frac{1}{2\pi^2 r}\int_0^\infty\mathrm{d}q\left(\frac{{\Lambda_\eta}^2}{{\Lambda_\eta}^2+q^2}\right)^2\frac{q\sin(qr)}{q^2+{m_\eta}^2}\right]\\
&= C_{\mathrm{p}\eta\bar{\mathrm{p}}}C_{\Omega\eta\bar{\Omega}}\left(\frac{{\Lambda_\eta}^2}{{\Lambda_\eta}^2-{m_\eta}^2}\right)^2\hat{\mathbb{S}}^i\hat{\sigma}^j\partial_i\partial_j\left[\frac{e^{-m_\sigma r}}{4\pi r}-\frac{e^{-\Lambda_\sigma r}}{4\pi r}+\frac{{m_\sigma}^2-{\Lambda_\sigma}^2}{8\pi\Lambda_\sigma}e^{-\Lambda_\sigma r}\right]\\
&= C_{\mathrm{p}\eta\bar{\mathrm{p}}}C_{\Omega\eta\bar{\Omega}}\left(\frac{{\Lambda_\eta}^2}{{\Lambda_\eta}^2-{m_\eta}^2}\right)^2\\
&\quad\left[\vec{\mathbb{S}}\cdot\vec{\sigma}\frac{1}{r}\frac{\mathrm{d}}{\mathrm{d}r}+(\vec{\mathbb{S}}\cdot\hat{r})(\vec{\sigma}\cdot\hat{r})\left(\frac{\mathrm{d}^2}{\mathrm{d}r^2}-\frac{1}{r}\frac{\mathrm{d}}{\mathrm{d}r}\right)\right]\left[\frac{e^{-m_\sigma r}}{4\pi r}-\frac{e^{-\Lambda_\sigma r}}{4\pi r}+\frac{{m_\sigma}^2-{\Lambda_\sigma}^2}{8\pi\Lambda_\sigma}e^{-\Lambda_\sigma r}\right]\\
&= \frac{C_{\mathrm{p}\eta\bar{\mathrm{p}}}C_{\Omega\eta\bar{\Omega}}}{3}\left(\frac{{\Lambda_\eta}^2}{{\Lambda_\eta}^2-{m_\eta}^2}\right)^2\\
&\quad\left[\vec{\mathbb{S}}\cdot\vec{\sigma}\nabla^2+\hat{O}_{\mathrm{T}}\left(\frac{\mathrm{d}^2}{\mathrm{d}r^2}-\frac{1}{r}\frac{\mathrm{d}}{\mathrm{d}r}\right)\right]\left[\frac{e^{-m_\sigma r}}{4\pi r}-\frac{e^{-\Lambda_\sigma r}}{4\pi r}+\frac{{m_\sigma}^2-{\Lambda_\sigma}^2}{8\pi\Lambda_\sigma}e^{-\Lambda_\sigma r}\right].
\end{aligned}\tag{2.81}$$

This calculation follows all of the operational development in last section. Therefore, the operators appearing in the potential are the same, but we have to substitute f function by

$$f(r)=\left(\frac{{\Lambda_\eta}^2}{{\Lambda_\eta}^2-{m_\eta}^2}\right)^2\left[\frac{e^{-m_\sigma r}}{4\pi r}-\frac{e^{-\Lambda_\sigma r}}{4\pi r}+\frac{{m_\sigma}^2-{\Lambda_\sigma}^2}{8\pi\Lambda_\sigma}e^{-\Lambda_\sigma r}\right],\tag{2.82}$$

to obtain the radial dependence.

All of the derivatives have been computed, in (2.45), except those for the exponential decay, so we label $g(r)=e^{-\Lambda_\eta r}$ and see, immediately,

$$\begin{aligned}
\frac{\mathrm{d}g}{\mathrm{d}r}&=-\Lambda_\eta e^{-\Lambda_\eta r},\\
\frac{\mathrm{d}^2g}{\mathrm{d}r^2}&={\Lambda_\eta}^2e^{-\Lambda_\eta r}.
\end{aligned}\tag{2.83}$$

Whereas the Laplacian was already computed in (2.49). Therefore, the final expression for the potential reads

$$\begin{aligned}
\hat{V}_\eta(\vec{r})=\frac{C_{\mathrm{p}\eta\bar{\mathrm{p}}}C_{\Omega\eta\bar{\Omega}}}{3}\left(\frac{{\Lambda_\eta}^2}{{\Lambda_\eta}^2-{m_\eta}^2}\right)^2\Bigg[&{m_\eta}^2\frac{e^{-m_\eta r}}{4\pi r}\left(\vec{\mathbb{S}}\cdot\vec{\sigma}+\left(1+\frac{3}{m_\eta r}+\frac{3}{(m_\eta r)^2}\right)\hat{O}_{\mathrm{T}}\right)\\
&-{\Lambda_\eta}^2\frac{e^{-\Lambda_\eta r}}{4\pi r}\left(\vec{\mathbb{S}}\cdot\vec{\sigma}+\left(1+\frac{3}{\Lambda_\eta r}+\frac{3}{(\Lambda_\eta r)^2}\right)\hat{O}_{\mathrm{T}}\right)\\
&+({m_\eta}^2-{\Lambda_\eta}^2)\frac{\Lambda_\eta r-2}{2}\frac{e^{-\Lambda_\eta r}}{4\pi r}\left(\vec{\mathbb{S}}\cdot\vec{\sigma}+\frac{\Lambda_\eta r+1}{\Lambda_\eta r-2}\hat{O}_{\mathrm{T}}\right)\Bigg].
\end{aligned}\tag{2.84}$$

As for the σ exchange potential, we must repeat the calculations for a somewhat easier transform. Following the last section,

$$\begin{aligned}
\hat{V}_\sigma(\vec{r}) &= -C_{\mathrm{p}\sigma\bar{\mathrm{p}}}C_{\Omega\sigma\bar{\Omega}}\int_{\mathbb{R}^3}\frac{\mathrm{d}\vec{q}}{(2\pi)^3}\frac{e^{\mathrm{i}\vec{q}\cdot\vec{r}}}{\vec{q}^{\,2}+{m_\sigma}^2}\left(F_{\Lambda_\sigma}(\vec{q})\right)^2 \\
&= -C_{\mathrm{p}\sigma\bar{\mathrm{p}}}C_{\Omega\sigma\bar{\Omega}}\int_{\mathbb{R}^3}\frac{\mathrm{d}\vec{q}}{(2\pi)^3}\frac{e^{\mathrm{i}\vec{q}\cdot\vec{r}}}{\vec{q}^{\,2}+{m_\sigma}^2}\left(\frac{{\Lambda_\sigma}^2}{{\Lambda_\sigma}^2+\vec{q}^{\,2}}\right)^2 \\
&= -C_{\mathrm{p}\sigma\bar{\mathrm{p}}}C_{\Omega\sigma\bar{\Omega}}\int_0^\infty\frac{\mathrm{d}q}{(2\pi)^2}\left(\frac{{\Lambda_\sigma}^2}{{\Lambda_\sigma}^2+q^2}\right)^2\frac{q^2}{q^2+{m_\sigma}^2}\int_{-1}^1\mathrm{d}\cos\theta\, e^{\mathrm{i}qr\cos\theta} \\
&= -\frac{C_{\mathrm{p}\sigma\bar{\mathrm{p}}}C_{\Omega\sigma\bar{\Omega}}}{2\pi^2 r}\int_0^\infty\mathrm{d}q\left(\frac{{\Lambda_\sigma}^2}{{\Lambda_\sigma}^2+q^2}\right)^2\frac{q\sin(qr)}{q^2+{m_\sigma}^2} \\
&= -C_{\mathrm{p}\sigma\bar{\mathrm{p}}}C_{\Omega\sigma\bar{\Omega}}\left(\frac{{\Lambda_\sigma}^2}{{\Lambda_\sigma}^2-{m_\sigma}^2}\right)^2\left[\frac{e^{-m_\sigma r}}{4\pi r}-\frac{e^{-\Lambda_\sigma r}}{4\pi r}+\frac{{m_\sigma}^2-{\Lambda_\sigma}^2}{8\pi\Lambda_\sigma}e^{-\Lambda_\sigma r}\right].
\end{aligned} \tag{2.85}$$

2.4 Potential parametrizations

Having built several functional forms for the effective potential, it is now time to give values to the remaining parameters so as to reproduce the behaviour of the pΩ potential. All things told, we have built a potential with a contact and an η exchange term, one with an added σ exchange term and one with form factors on the exchange terms.

Since our parametrizations will be fit to elastic channels, we should write the final expression for the elastic channel contributions, with cut-off $\delta = \sqrt{2}/m_\omega$,

$$\begin{aligned}
\hat{V}_{\mathrm{ct}}^{\mathrm{el}} &= \left(C_0^0 + C_0^1\vec{\mathbb{S}}\cdot\vec{\sigma}\right)\frac{e^{-(r/\delta)^2}}{\pi^{3/2}\delta^3}, \\
\hat{V}_\eta^{\mathrm{el}} &= C_{\mathrm{p}\eta\bar{\mathrm{p}}}C_{\Omega\eta\bar{\Omega}}\frac{{m_\eta}^2}{3}\left(\frac{{\Lambda_\eta}^2}{{\Lambda_\eta}^2-{m_\eta}^2}\right)^2\left[\frac{e^{-m_\eta r}}{4\pi r}-\frac{e^{-\Lambda_\eta r}}{4\pi r}+\frac{({m_\eta}^2-{\Lambda_\eta}^2)\Lambda_\eta}{8\pi{m_\eta}^2}e^{-\Lambda_\eta r}\right]\vec{\mathbb{S}}\cdot\vec{\sigma}, \\
\hat{V}_\sigma^{\mathrm{el}} &= -C_{\mathrm{p}\sigma\bar{\mathrm{p}}}C_{\Omega\sigma\bar{\Omega}}\left(\frac{{\Lambda_\sigma}^2}{{\Lambda_\sigma}^2-{m_\sigma}^2}\right)^2\left[\frac{e^{-m_\sigma r}}{4\pi r}-\frac{e^{-\Lambda_\sigma r}}{4\pi r}+\frac{{m_\sigma}^2-{\Lambda_\sigma}^2}{8\pi\Lambda_\sigma}e^{-\Lambda_\sigma r}\right].
\end{aligned} \tag{2.86}$$

2.4.1 $^5S_2$ potential fitting

For all of these potentials, we have two free parameters for the contact term, C_0^0 and C_0^1. Adding the σ exchange adds an extra $C_{\Omega\sigma\bar{\Omega}}$ parameter. Adding the form factors adds two cutoffs, Λ_η and Λ_σ. We will take the choices for these parameters by fixing some and then fitting the rest to

$$V(r) = b_1 e^{-b_2 r^2} + b_3\left(1-e^{-b_4 r^2}\right)\left(\frac{e^{-m_\pi}}{r}\right)^2, \tag{2.87}$$

the HAL QCD potential for the $^5S_2$ channel with $t/a = 12$ and $n = 1$, which has constants [IA+19]

$$\begin{aligned}
b_1 &= -313.0\,\mathrm{MeV}, \\
b_2 &= 81.7\,\mathrm{fm}^{-2}, \\
b_3 &= -252\,\mathrm{MeV}\cdot\mathrm{fm}^2, \\
b_4 &= 0.85\,\mathrm{fm}^{-2}.
\end{aligned} \tag{2.88}$$

This potential is itself a fit of the lattice potential. For us, it will be the "real" potential, which we will fit with our effective potential.

	$C_0^0(\mathrm{MeV}^{-2})$	$C_0^1(\mathrm{MeV}^{-2})$	$C_{\Omega\sigma\bar{\Omega}}$	$\Lambda_\eta(\mathrm{MeV})$	$\Lambda_\sigma(\mathrm{MeV})$
Florit	$5.00 \cdot 10^{-3}$	$1.00 \cdot 10^{-3}$			
Reduced Florit	$1.25 \cdot 10^{-3}$	$0.25 \cdot 10^{-3}$			
No FF	$-8.06(6) \cdot 10^{-6}$	$-1.61(2) \cdot 10^{-6}$	0.8858(2)		
Fixed FF	$1.133(5) \cdot 10^{-5}$	$2.267(9) \cdot 10^{-6}$	1.882(8)	900	1200
Free FF	$6.59(6) \cdot 10^{-6}$	$1.32(2) \cdot 10^{-6}$	2.58(3)	917.4(7)	622(6)

Table 2: Parameter choices taken. The blank squares correspond to constants not in the model.

Both Florit sets are taken from [Flo14] and include only the contact and η exchange terms. The Florit set corresponds to a reasonable guess in the sense that it is close to the $S = -1$ and $S = -2$ sectors, shown in table 3 for completeness, whereas the reduced Florit set corresponds to the expectation that this interaction be weaker.

	$C_0^0(\mathrm{MeV}^{-2})$	$C_0^1(\mathrm{MeV}^{-2})$
$N\Lambda \to N\Lambda$	$5.7 \cdot 10^{-3}$	$1.2 \cdot 10^{-3}$
$N\Sigma \to N\Sigma$	$5.6 \cdot 10^{-3}$	$1.3 \cdot 10^{-3}$
$N\Xi \to N\Xi$	$4.8 \cdot 10^{-3}$	$9.9 \cdot 10^{-4}$

Table 3: Experimental results for the contact constants for some $S = -1$ and $S = -2$ channels [Flo14, PHM07, HP+13].

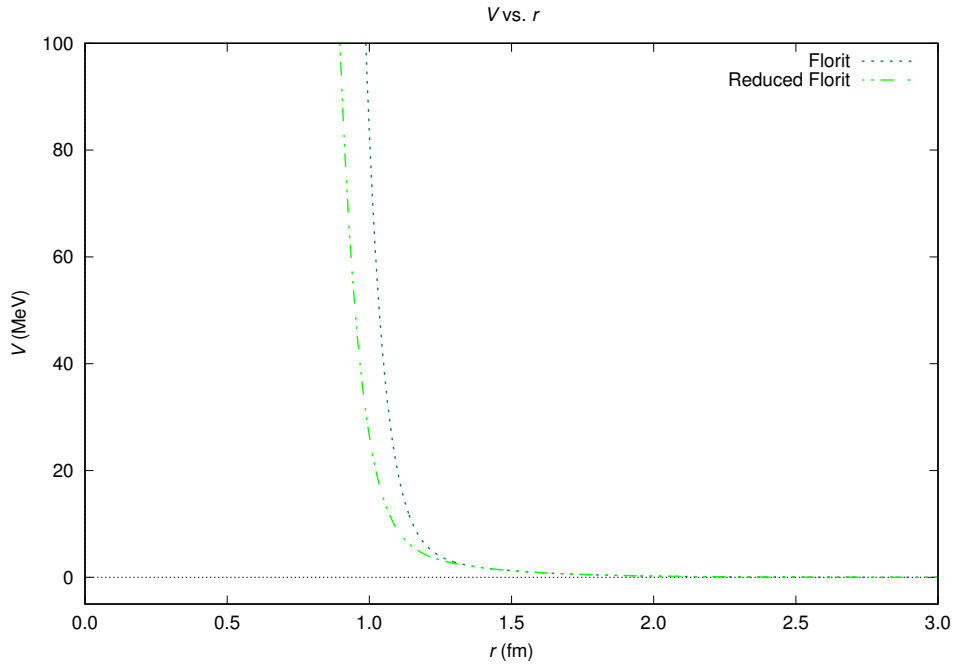

Figure 9: pΩ potential for the ${}^5S_2$ channel, according to the Florit choices.

Both of them, however, are very repulsive, which stands in stark contrast with the attractiveness of the HAL QCD potential. We will still study these potentials through the rest of the work anyway, since we are interested in seeing how the scattering and femtoscopy observables behave under this very repulsive limiting case.

As for the "no form factor" and "free form factors" fits, they are taken by a minimum squares fit to the HAL QCD potential computed using a Python script, the first without form factors and the second with form factors. The "fixed form factors" fit is obtained by fixing the Λ_η and Λ_σ constants to

a reasonable physical value (see table 2) and taking a minimum squares fit to the HAL QCD potential on the remaining three constants.

It is interesting to notice that, while the "no form factor" fit loses the repulsive behaviour of the contact interaction we found in the $S = -1$ and $S = -2$ sectors, the "fixed form factors" and "free form factors" parametrizations do keep the contact interaction repulsive.

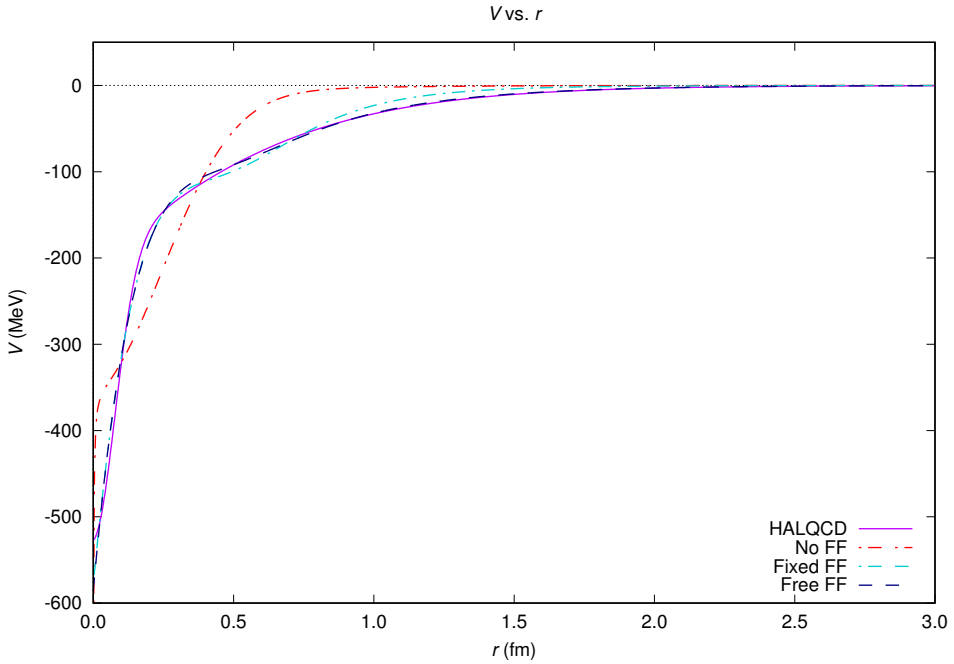

Figure 10: $p\Omega$ potential for the ${}^5S_2$ channel, according to the fit choices.

In all cases, we have made the guess that $C_0^0 = 5C_0^1$. A guess is needed due to the fact that these two constants are not separable within the ${}^5S_2$ channel, and we have no potential for the ${}^3S_1$ channel with which we can fix them. This guess is, again, based on the behaviour of the constants for the $S = -1$ and $S = -2$ sectors.

We see that the "no form factor" parametrization differs importantly from the HAL QCD potential. Therefore, we are not going to consider it for the rest of the work.

On the contrary, we observe a very faithful behaviour of the "free form factors" fit. When giving physical meaning to the form factors, however, we find the problem that $\Lambda_\sigma = 622$ MeV, while for scalar couplings we would expect $\Lambda_\sigma \sim 1.2$ MeV (as in table 2). This should not be cause for concern: the form factor will begin to modify the potential at $|\vec{q}| \sim 600$ MeV. However, since $m_\sigma = 500$ MeV, the relativistic corrections will be relevant already, and we have not considered them. Hence, there is a systematic error we cannot control within our model, which explains the unexpectedly low value for Λ_σ.

2.4.2 ${}^5S_2$ bound states

As commented, the $N\Omega$ pairs are candidates for dibaryons. Therefore, it is interesting to try if the developed potentials admit any bound states. For this matter, a numerical method has been implemented in Fortran 90 (see section A.1) to compute such states by solving the Schrödinger radial equation,

$$\left[\frac{\mathrm{d}^2}{\mathrm{d}r^2} + k^2 - \frac{2\mu Z_1 Z_2 \alpha}{r} - 2\mu\hat{V}(r) - \frac{l(l+1)}{r^2}\right] u_l(r) = 0, \tag{2.89}$$

which allows us to obtain the radial behaviour of the wave function in the case of central potentials and where $k^2 = 2\mu E$, E is the energy, μ is the reduced mass, Z_1 and Z_2 are the charges of each particles

and l is the angular momentum number. The development of this equation will be further discussed in the following section.

Using said code, one finds no bound state for the Florit potentials (which is to be expected, as they are very repulsive). One does find bound states for the "form factors" (FF) fit potentials, as well as for the HAL QCD potential, all of which with $l = 0$.

	$p\Omega$		$n\Omega$	
	$E(\mathrm{MeV})$	$\sqrt{\langle r^2\rangle}(\mathrm{fm})$	$E(\mathrm{MeV})$	$\sqrt{\langle r^2\rangle}(\mathrm{fm})$
HAL QCD	-2.26	3.40	-1.38	3.99
Fixed form factors	-0.428	7.59	$-3.65 \cdot 10^{-3}$	18.9
Free form factors	-2.13	3.47	-1.26	4.13

Table 4: Energy and mean squared radius of a ${}^5S_2$ bound state obtained for all potential choices that admit one.

The $n\Omega$ case has been obtained simply by assuming isospin symmetry and using the same $p\Omega$ potential not including the Coulomb interaction.

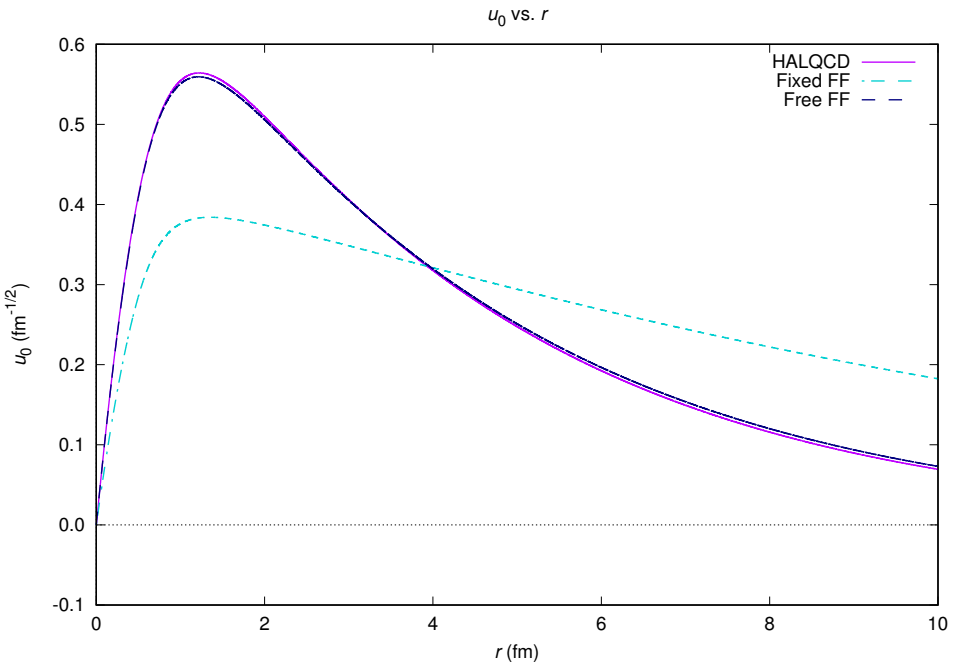

Figure 11: Radial wave function of the bound states of the $p\Omega$ interaction as built with the different potential choices in the ${}^5S_2$ channel.

We find most similarity, as is to be expected, in the wave functions of the HAL QCD and its best fit, the "free form factors" fit.

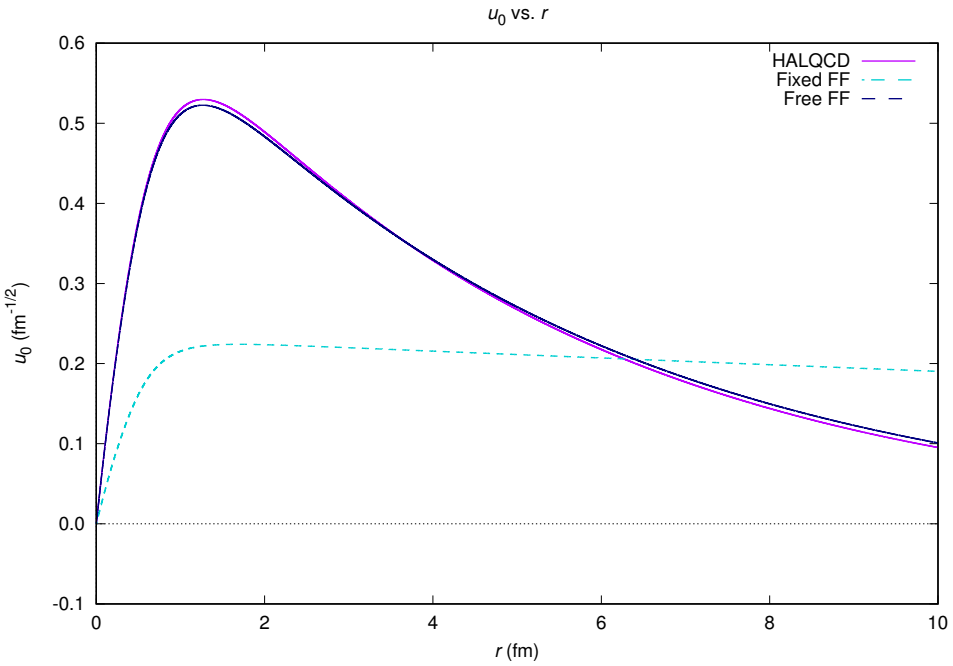

Figure 12: Radial wave function of the bound states of the $n\Omega$ interaction as built with the different potential choices for the ${}^5S_2$ channel.

We observe the same general behaviour for the neutron and proton cases, although the states are predictably less bound for the neutron case.

2.4.3 ${}^3S_1$ potential and bound states

The parametrizations given so far, under the $C_0^0 = 5C_0^1$ assumption, allow us to also give a form to the ${}^3S_1$ potential.

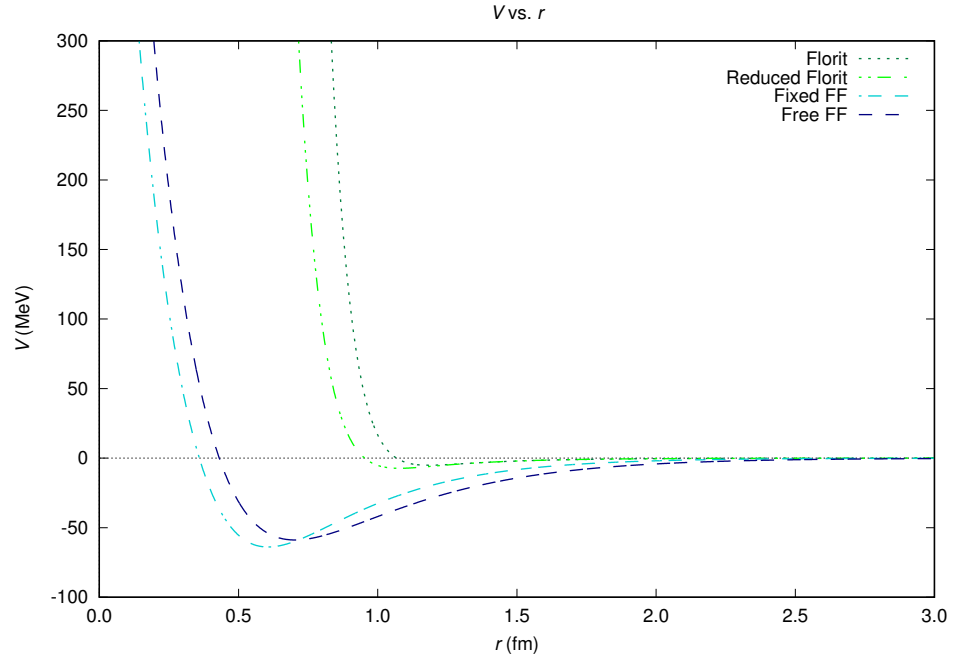

Figure 13: $p\Omega$ potential for the ${}^3S_1$ channel.

From the figure, one can already suppose there is only a bound state for the "fixed form factors" and "free form factors" choices, since the Florit parametrizations yield only a much too small minimum. The program yields exactly these expected results.

	pΩ		nΩ	
	$E(\mathrm{MeV})$	$\sqrt{\langle r^2\rangle}(\mathrm{fm})$	$E(\mathrm{MeV})$	$\sqrt{\langle r^2\rangle}(\mathrm{fm})$
Fixed form factors fit	$-5.45 \cdot 10^{-2}$	27.9		
Free form factors fit	$-4.81 \cdot 10^{-1}$	6.91	$-7.69 \cdot 10^{-2}$	13.6

Table 5: Energy and mean squared radius of a $^3S_1$ bound state obtained for all potential choices that admit one.

We see that, for the pΩ case, the "fixed form factors" choice just barely generates a bound state, with a very large radius, whereas the "free form factors" fit does give a somewhat more stable state.

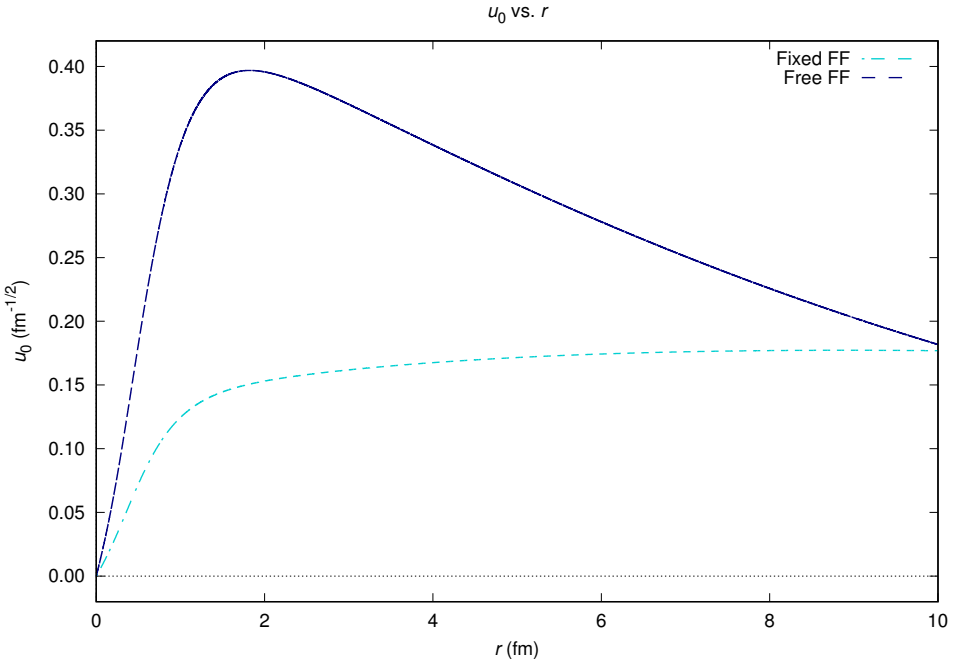

Figure 14: Radial wave function of the bound states of the pΩ interaction as built with the different potential choices in the $^3S_1$ channel.

As for the nΩ case, the "fixed form factors" fit is no longer able to support the bound state, and the "free form factors" fit barely so. Therefore, we find only one bound state left, and with very small binding energy.

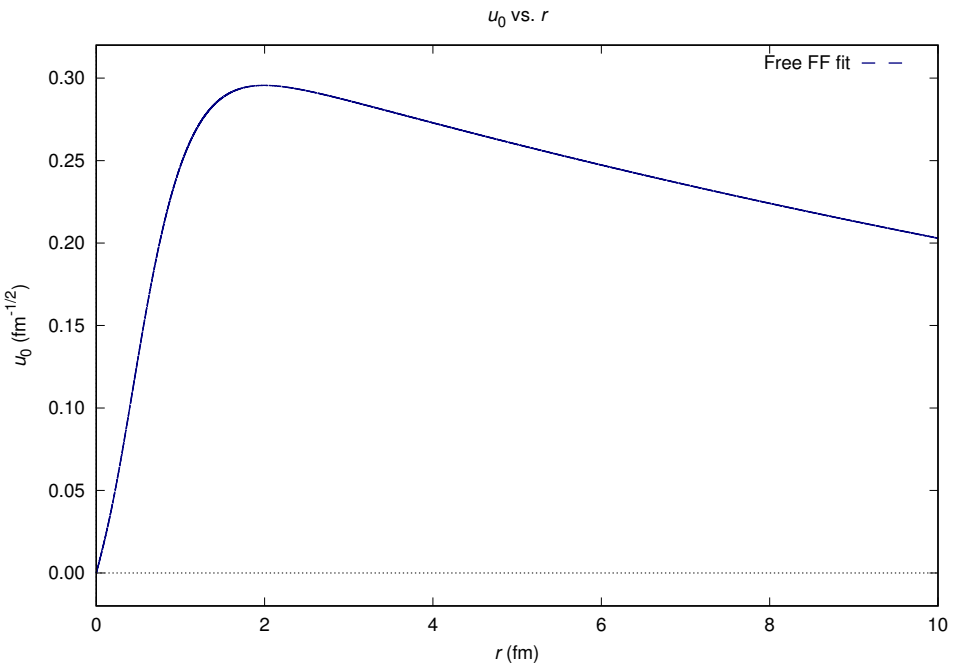

Figure 15: Radial wave function of the bound states of the $\mathrm{n}\Omega$ interaction as built with the different potential choices in the $^3S_1$ channel.

3 Scattering under the $N\Omega$ potential

Having obtained a potential for the $N\Omega$ interaction, our next step is to understand the way its scattering wave functions (that is, unbound solutions of the Schrödinger equation) will be built. To do so, we will introduce the fundamentals of scattering theory and then compute the wave functions for the potentials [MM23, Joa75].

3.1 Scattering on local potentials

By scattering we refer to the process in which one object interacts with another. Generally, one considers one of the objects as being scattered, whereas the other is treated as a scattering center, usually represented by a scattering potential.

In the case of a two-body collision, we can work in the center of mass reference frame with relative coordinates. Therefore, the general theory of scattering for one scattering particle and a scattering potential may also be used using the reduced mass μ instead of the particle masses and using relative coordinates.

In the quantum case, therefore, scattering is described as the transition from one quantum state to another. We consider, hence, the initial state $|\mathrm{i}\rangle$ to be that of a free particle, that is, a plane wave with momentum $\vec{k}$. Hence, for the free-particle Hamiltonian $\hat{H}_0$, we have

$$\hat{H}_0 \left|\mathrm{i}\right\rangle = \frac{k^2}{2\mu} \left|\mathrm{i}\right\rangle . \tag{3.1}$$

Scattering is introduced by the action of a potential $\hat{V}$ on a finite range R. One works, hence, with the Hamiltonian $\hat{H} = \hat{H}_0 + \hat{V}(\vec{r})$, and tries to understand the action of $\hat{H}$ on the free-particle initial state $|\mathrm{i}\rangle$.

We suppose, then, the particle inside a cubic box of side L. Then, the free particle is represented by

$$\begin{aligned} \left\langle \vec{r} \mid \vec{k} \right\rangle &= \frac{e^{\mathrm{i}\vec{k}\cdot\vec{r}}}{L^{3/2}} \\ &= N e^{\mathrm{i}\vec{k}\cdot\vec{r}}. \end{aligned} \tag{3.2}$$

At the end of the calculation, we will take $L \to \infty$ to reproduce the continuum character of the state. Given that the scattering potential be real and local, we get the asymptotic behaviour

$$\psi(\vec{r}) \xrightarrow{r \gg R} N \left[e^{\mathrm{i}\vec{k}\cdot\vec{r}} + \frac{e^{\mathrm{i}kr}}{r} f(\vec{k}', \vec{k}) \right] . \tag{3.3}$$

Thus, the wave function becomes a combination of the incident plane wave and a spherical wave, modulated by a function f, the scattering amplitude, which depends on the initial and final momenta, $\vec{k}$ and $\vec{k}'$, and has the form

$$f(\vec{k}', \vec{k}) = -\frac{\mu L^3}{2\pi} \int_{\mathbb{R}^3} \left\langle \vec{k}' \mid \vec{r}' \right\rangle \hat{V}(\vec{r}') \left\langle \vec{r}' \mid \psi \right\rangle \mathrm{d}\vec{r}' . \tag{3.4}$$

Assuming that the potential also shows spherical symmetry, we may write $\hat{V}(\vec{r}) = \hat{V}(r)$. Hence, in the scattering region, $0 < r < R$, we get the Schrödinger equation

$$-\frac{1}{2\mu}\nabla^2\psi + \hat{V}(r)\psi = E\psi. \tag{3.5}$$

The total energy is $E = k^2/2\mu$, since the scattering process is elastic. The wave function shows dependency on r, the scattering angle θ and $\vec{k}$, so we write $\varphi(r, \theta)$. We take the coordinates so that $\vec{k}\cdot\vec{r} = kz$ and we may, thus, write the asymptotic behaviour as

$$\psi(r, \theta) \xrightarrow{r \gg R} N \left[e^{\mathrm{i}kz} + \frac{e^{\mathrm{i}kr}}{r} f(\theta) \right] . \tag{3.6}$$

3.1.1 Partial waves expansion

Considering a potential with the specified assumptions, we need to build a complete set of eigenfunctions. We may write the Hamiltonian in spherical coordinates, which yields the eigenvalue equation

$$\left[-\frac{1}{2\mu r}\frac{\partial^2}{\partial r^2}\hat{r} + \frac{\hat{L}^2}{2\mu r^2} + \hat{V}(r)\right]\chi(r,\theta,\varphi) = E\chi(r,\theta,\varphi). \tag{3.7}$$

Since the operators $\hat{H}$, $\hat{L}^2$ and $\hat{L}_z$ commute, we may build a complete set of eigenfunctions characterized by their eigenvalues, E, $l(l+1)$ and m respectively, that is,

$$\begin{aligned}\hat{H}\chi &= E\chi,\\ \hat{L}^2\chi &= l(l+1)\chi,\\ \hat{L}_z\chi &= m\chi.\end{aligned} \tag{3.8}$$

We propose a separable solution of the form

$$\chi(r,\theta,\varphi) = \frac{u_l(r)}{r}Y_{lm}(\theta,\varphi), \tag{3.9}$$

where u_l are radial functions and Y_{lm} are the spherical harmonics. By introducing this in the Schrödinger equation (eq. (3.7)), we obtain an equation for u_l depending only on the radial coordinate,

$$\left[\frac{\mathrm{d}^2}{\mathrm{d}r^{\,2}} + k^2 - 2\mu\hat{V}(r) - \frac{l(l+1)}{r^2}\right]u_l(r) = 0. \tag{3.10}$$

We require that χ is finite at the origin, hence we need to impose $u_l(0) = 0$. Since the particle is free for $r > R$, on the other hand, the solution is a combination of the spherical Bessel functions of the first and second kind, j_l and n_l,

$$u_l(r) = r(c_l' j_l(kr) + c_l'' n_l(kr)). \tag{3.11}$$

It is more practical, however, to write them in terms of the spherical Hankel functions of the first and second kind, given by $h_l^1(x) = j_l(x) + \mathrm{i}n_l(x)$ and $h_l^2(x) = j_l(x) - \mathrm{i}n_l(x)$, as

$$u_l(r) = r(c_l^1 h_l^1(kr) + c_l^2 h_l^2(kr)). \tag{3.12}$$

We know, though, that the solution for a non scattered free particle (that is, a plane wave), is given by $e^{\mathrm{i}kr\cos\theta}$ and contains components with all possible values of l, as given by Rayleigh's formula,

$$e^{\mathrm{i}kr\cos\theta} = \sum_{l=0}^{\infty}\mathrm{i}^l(2l+1)j_l(kr)P_l(\cos\theta), \tag{3.13}$$

where P_l are the Legendre polynomials. We see there is no dependency on φ, as we expect by the asymptotic behaviour discussed in the earlier section.

Using the asymptotic behaviour of spherical Hankel functions, we get the expansion for the Rayleigh formula,

$$e^{ikr\cos\theta} \xrightarrow{r\gg R} \sum_{l=0}^{\infty}\frac{2l+1}{2\mathrm{i}kr}[e^{\mathrm{i}kr} - (-1)^l e^{-\mathrm{i}kr}]P_l(\cos\theta). \tag{3.14}$$

This behaviour suggests that we may write the solution for $r > R$ as

$$\psi(r,\theta) = N\sum_{l=0}^{\infty}\mathrm{i}^l(2l+1)\frac{u_l(r)}{r}P_l(\cos\theta). \tag{3.15}$$

Its asymptotic behaviour, substituting the expression of u_l with Hankel functions, is written as

$$\psi(r,\theta) \xrightarrow{r\gg R} N\sum_{l=0}^{\infty}\frac{2l+1}{\mathrm{i}kr}[c_l^1 e^{\mathrm{i}kr} - (-1)^l c_l^2 e^{-\mathrm{i}kr}]P_l(\cos\theta). \tag{3.16}$$

3.1.2 Phase shifts

Taking $N = 1$ and $c_l^1 = c_l^2 = 1/2$ we recover the non scattered case, which is also evident as this choice gets back to the free particle case $u_l(r) = rj_l(kr)$. This situation occurs whenever we take $c_l^1 = c_l^2$ (and of course setting the normalizing constant N to the appropriate value). Therefore, what is relevant is the two coefficients ratio, which may be written as

$$\frac{c_l^1}{c_l^2} = e^{2\mathrm{i}\delta_l}, \tag{3.17}$$

where δ_l is called phase shift, and is obviously dependant on k. We may now express the same behaviour depending on this new quantity,

$$\psi(r,\theta) \xrightarrow{r\gg R} N\sum_{l=0}^{\infty} \frac{2l+1}{\mathrm{i}kr} c_l[e^{2\mathrm{i}\delta_l}e^{\mathrm{i}kr} - (-1)^l e^{-\mathrm{i}kr}]P_l(\cos\theta). \tag{3.18}$$

One can identify in this expression the scattering amplitude, which is then written as

$$f(\theta) = \sum_{l=0}^{\infty}(2l+1)\frac{e^{2\mathrm{i}\delta_l}-1}{2ik}P_l(\cos\theta). \tag{3.19}$$

We refer to the factor $e^{2\mathrm{i}\delta_l}/2\mathrm{i}k$ as the partial wave scattering amplitude, f_l.

As for physical meaning, using the asymptotic behaviour we see that δ_l is, in fact, the difference between the phase of the wave function and that of the incident wave. In the non scattered situation, we get $\delta_l = 0$, which yields a free particle solution for all space. Since, for $r > R$, we have a free particle, the phase shift δ_l is the result of the interaction that the particle experimented when $r < R$.

Using the definition of the phase shift, we may write the radial part of the wave function in the region $r > R$,

$$\begin{aligned} u_l(r) &= \frac{r}{2}[e^{2\mathrm{i}\delta_l}h_l^1(kr) + h_l^2(kr)] \\ &= re^{\mathrm{i}\delta_l}[\cos\delta_l j_l(kr) - \sin\delta_l n_l(kr)]. \end{aligned} \tag{3.20}$$

This way, the mathematical description of the situation is given exclusively by the phase shift, which reduces the problem to calculating just this quantity.

As for calculating the phase shift, we may obtain it in terms of the dimensionless logarithmic derivative at $R^- = R - \varepsilon$ (for some small $\varepsilon \in \mathbb{R}^+$), $\beta_l = Ru_l'(R)/u_l(R)$, by equating it to the known expression for $R^+ = R + \varepsilon$, which yields

$$\cot\delta_l = \frac{kRn_l'(kR) - (\beta_l - 1)n_l(kR)}{kRj_l'(kR) - (\beta_l - 1)j_l(kR)}. \tag{3.21}$$

There is one last piece of information we can obtain from the phase shifts which is of interest at the moment. It is a known result of quantum scattering theory that, for spherical potentials V such that

$$\int_0^{\infty} \mathrm{d}r\, r|V(r)| < \infty, \tag{3.22}$$

the phase shift behaves like

$$\delta_l(0) - \delta_l(\infty) = \begin{cases} (n_l + 1/2)\pi & \text{if there is a half-bound state, and} \\ n_l\pi & \text{otherwise,} \end{cases} \tag{3.23}$$

where n_l is the number of bound states with relative momentum number l. We call a state "half bound" if its wave function decays to zero but not fast enough to be square integrable. [Zho06] By obtaining the phase shifts, therefore, we should be able to determine if there are bound states. We already did that in last section, so in this case this is just a consistency check.

3.2 $n\Omega$ scattering

Having developed the formalism for short-range scattering, we may now compute the scattering wave functions for the Coulomb-less potentials in last section and study them. In order to do so, we build the solutions of the wave function for the potentials with a Fortran 90 code (see section A.2).

3.2.1 $n\Omega$ scattering wave functions in the $^5S_2$ channel

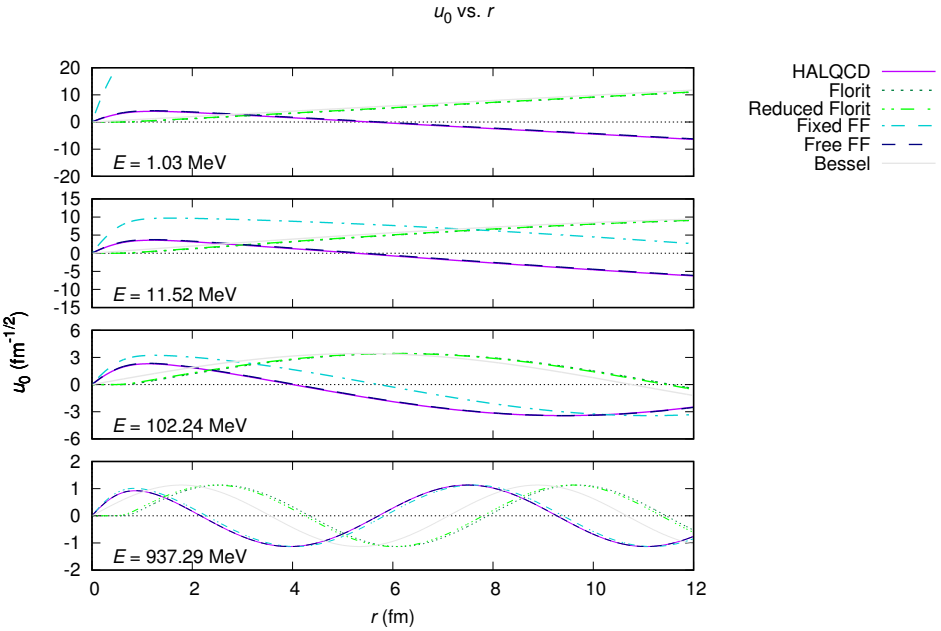

Figure 16: Radial wave functions for various energies, obtained using last section's potentials for the $^5S_2$ $n\Omega$ channel.

One may observe, in the wave function profiles, the expected similarity between those obtained by the HAL QCD potential and the "free form factors" fit potential, as well as a qualitatively similar, yet quantitatively distant, behaviour for the "fixed form factors" fit wave. As for the Florit potentials, their very repulsive core explains the constant-like behaviour they have at very small radii.

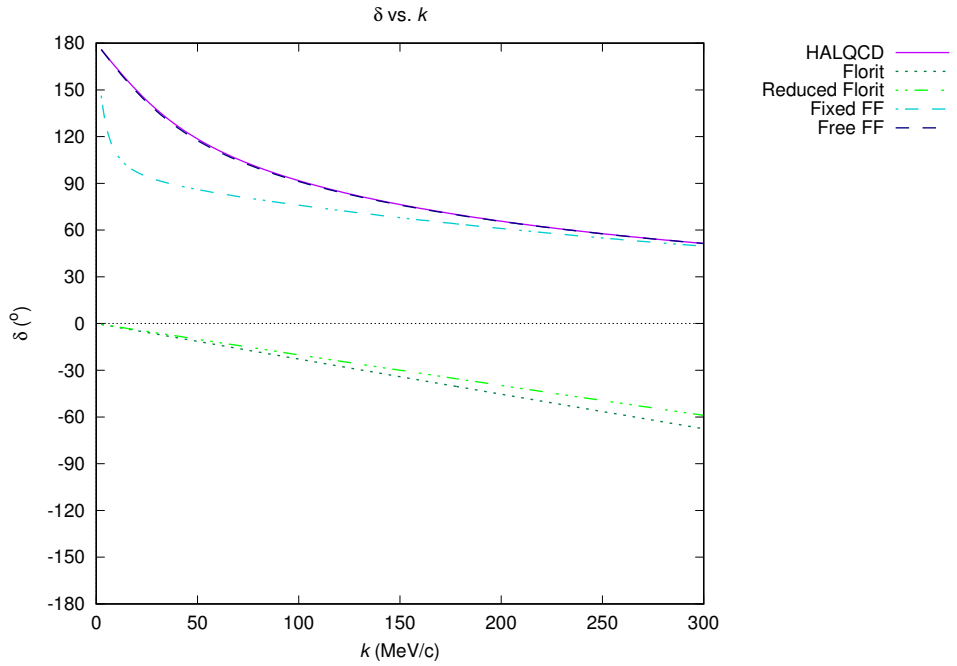

Figure 17: Phase shifts for the ${}^5S_2$ nΩ channel, obtained using the potentials discussed in section 1.

The behaviour explained in the last paragraph can also be interpreted in terms of phase shifts. Notably, by the Levinson theorem, the fact that all potentials start at $180°$, except for the Florit parametrizations, is a sign of the presence of a bound state for those potentials. This is in agreement with the bound states we found in section 1.

3.2.2 nΩ scattering wave functions in the ${}^3S_1$ channel

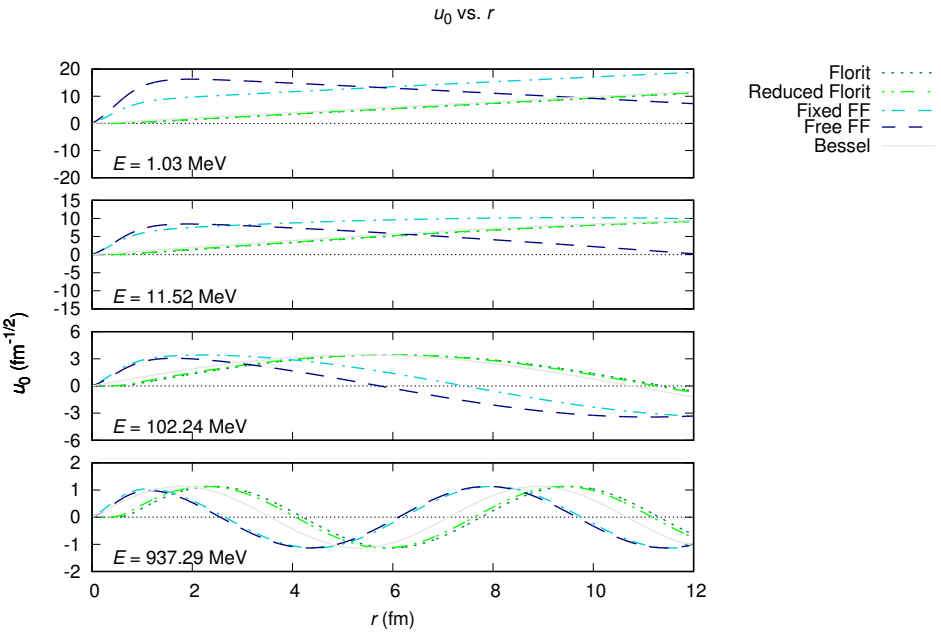

Figure 18: Radial wave functions for various energies, obtained using last section's potentials for the ${}^3S_1$ nΩ channel.

We again observe the predictable more moderate behaviour of the form factor potentials and the effect of the hard repulsive core of the Florit parametrizations.

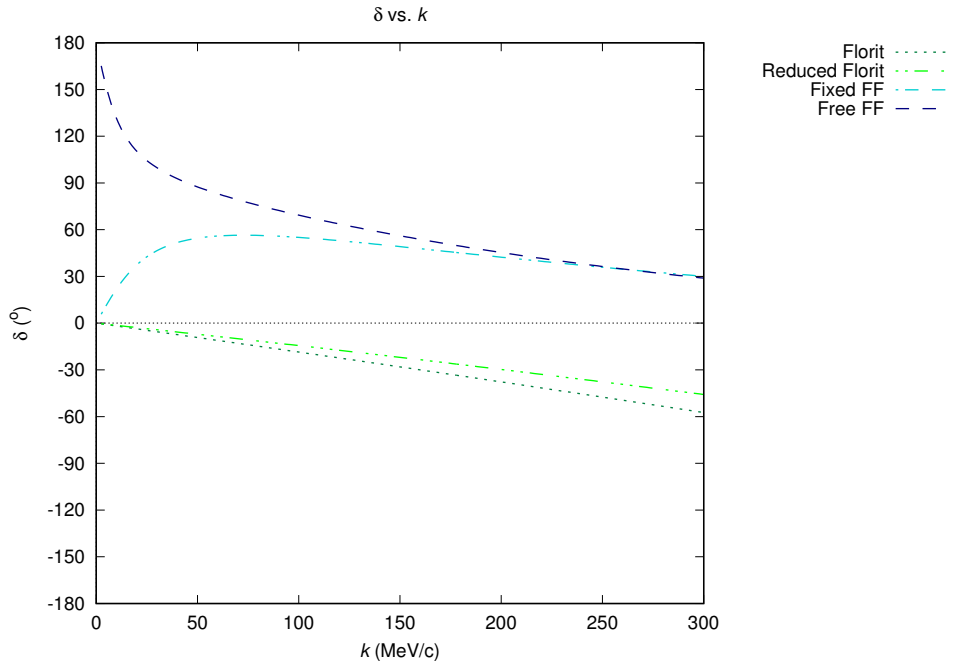

Figure 19: Phase shifts for the ${}^3S_1$ nΩ channel, obtained using last section's potentials.

In this case, we see that the "fixed form factors" parametrization gets a phase shift starting at $0°$. This does indicate, again by the Levinson theorem, that it does not admit a bound state, whereas the "free form factors" parametrization still does. This, again, is in agreement with the bound states found in last section.

3.3 Scattering under Coulomb interaction

The Coulomb potential, due to its characteristic slow r^{-1} decrease, cannot be treated locally. Therefore, it may not be directly analyzed with the scattering theory we built for local potentials.

However, the Schrödinger equation for particles subject to the Coulomb potential is analytically solvable. Hence, we may build the scattering theory atop the Coulomb wave functions instead of the free particle wave functions. Then, we treat the local potential the same way we did for the free particle case.

This will result in a very similar expression for the various features of the system, in particular for the wave function and the phase shifts, in which we will only exchange the spherical Bessel functions (which correspond to the free particle case) for the functions which characterize the Coulomb scattering [MM23, Joa75].

3.3.1 Analytical solution for the Coulomb potential

As said previously, we need the wave functions for the Coulomb potential alone, which will yield the asymptotic behaviour of the scattered solutions (again with a phase shift). Although one may be tempted to solve the Schrödinger equation in spherical coordinates (given the fact that the Coulomb potential does have spherical symmetry), it will be easier to solve the equation in parabolic coordinates, that is, given by

$$\begin{cases} \xi = r(1+\cos\varphi), \\ \eta = r(1-\cos\varphi), \\ \varphi = \arctan y/x. \end{cases} \tag{3.24}$$

Said coordinates are called "parabolical" due to the fact that the surfaces with constant ξ or η are paraboloids of revolution. In this system, the Laplacian operator is written

$$\nabla^2 = \frac{4}{\xi+\eta}\left[\frac{\partial}{\partial\xi}\left(\xi\frac{\partial}{\partial\xi}\right)+\frac{\partial}{\partial\eta}\left(\eta\frac{\partial}{\partial\eta}\right)\right]+\frac{1}{\xi\eta}\frac{\partial^2}{\partial\varphi^2}. \tag{3.25}$$

Hence, the Schrödinger equation takes the form

$$-\frac{2}{\mu(\xi+\eta)}\left[\frac{\partial}{\partial\xi}\left(\xi\frac{\partial\psi}{\partial\xi}\right)+\frac{\partial}{\partial\eta}\left(\eta\frac{\partial\psi}{\partial\eta}\right)\right]+\frac{2Z_1Z_2\alpha}{\xi+\eta}\psi = E\psi, \tag{3.26}$$

where α is the fine structure constant and Z_1, Z_2 are the charges of the scattered particle and the scattering center in units of e. Notice that we have not included the derivative with respect to φ, since the solution needs to exhibit azimuthal symmetry. Hence, we may propose a product solution $\psi(\xi,\eta) = f(\xi)g(\eta)$, which yields two different equations,

$$\begin{aligned}\frac{\mathrm{d}}{\mathrm{d}\xi}\left(\xi\frac{\mathrm{d}f}{\mathrm{d}\xi}\right)+[(k/2)^2\xi-\nu_1]f = 0,\\ \frac{\mathrm{d}}{\mathrm{d}\eta}\left(\eta\frac{\mathrm{d}g}{\mathrm{d}\eta}\right)+[(k/2)^2\xi-\nu_2]g = 0,\end{aligned} \tag{3.27}$$

where $k=\sqrt{2\mu E}$ and ν_1,ν_2 are such that $\nu_1+\nu_2=\gamma k$, and we have defined $\gamma=\mu Z_1Z_2\alpha/k$. If we take $\nu_1 = \mathrm{i}k/2$, we see that

$$f(\xi) = e^{\mathrm{i}k\xi/2} \tag{3.28}$$

is a solution for its differential equation. Then, we may define a new function h such that $g(\eta) = e^{-\mathrm{i}k\eta/2}h(\eta)$, and get the differential equation

$$\eta\frac{\mathrm{d}^2h}{\mathrm{d}\eta^2}+(1-\mathrm{i}k\eta)\frac{\mathrm{d}h}{\mathrm{d}\eta}-\gamma kh = 0, \tag{3.29}$$

which is known as the Kummer-Laplace equation, and has solution

$$h(\eta) = C\,{}_1F_1(-\mathrm{i}\gamma;1;\mathrm{i}k\eta), \tag{3.30}$$

where ${}_1F_1$ is the confluent hypergeometric function.

This finishes the job, since now we only need to put all of these results together and return to spherical coordinates, which yields the solution

$$\psi(r,\theta,\varphi) = e^{-\pi\gamma/2}\Gamma(1+\mathrm{i}\gamma)e_1^{\mathrm{i}kr\cos\theta}F_1(-\mathrm{i}\gamma;1;\mathrm{i}kr(1-\cos\theta)). \tag{3.31}$$

The value for C gets fixed by imposing the condition that we get probability density one in the configuration space.

3.3.2 Partial waves expansion for the Coulomb potential

Now that we have the solution for the Coulomb potential, we will perform the partial waves expansion, which will be useful, like in the free particle case, to understand the effect of the local potential. To do so, we write the Schrödinger equation in spherical coordinates,

$$\left[-\frac{1}{2\mu r}\frac{\partial^2}{\partial r^2}\hat{r}+\frac{\hat{L}^2}{2\mu r^2}+\frac{Z_1Z_2\alpha}{r}\right]\chi(r,\theta,\varphi) = E\chi(r,\theta,\varphi). \tag{3.32}$$

Again, the operators $\hat{H}$, $\hat{L}^2$ and $\hat{L}_z$ commute, so χ will again be eigenfunctions of said operators.

Also as we did for the free particle case, we propose a separable solution of the form

$$\chi(r,\theta,\varphi) = \frac{u_l(r)}{r} Y_{lm}(\theta,\varphi), \tag{3.33}$$

and get the same radial Schrödinger equation, this time for the particular case of the Coulomb potential,

$$\left[\frac{\mathrm{d}^2}{\mathrm{d}r^2} + k^2 - \frac{2\mu Z_1 Z_2 \alpha}{r} - \frac{l(l+1)}{r^2}\right] u_l(r) = 0. \tag{3.34}$$

We now set the axes, again, so that $\vec{r}\cdot\vec{k} = rz$, that is, we get the z axis in the direction and sense of the $\vec{k}$ wave vector. If we substitute $u_l(r) = e^{\mathrm{i}kr}(kr)^{l+1}v_l(-2\mathrm{i}kr)$ and perform the change of variables $\xi = -2\mathrm{i}kr$, the radial equation becomes

$$\xi\frac{\mathrm{d}^2 v_l}{\mathrm{d}r^2} + (2l+2-\xi)\frac{\mathrm{d}v_l}{\mathrm{d}\xi} - (l+1+\mathrm{i}\gamma)v_l = 0, \tag{3.35}$$

We recognize, again, the Kummer-Laplace equation, and obtain the solution

$$v_l(r) = C_{l1}F_1(l+1+\mathrm{i}\gamma; 2l+2; -2\mathrm{i}kr). \tag{3.36}$$

Then, the expression for u_l is the function known as regular spherical Coulomb function, F_l,

$$\begin{aligned} u_l(r) &= F_l(k,r) \\ &= C_l e^{\mathrm{i}kr}(kr)^{l+1}_1F_1(l+1+\mathrm{i}\gamma; 2l+2; -2\mathrm{i}kr). \end{aligned} \tag{3.37}$$

We still need to obtain the C_l coefficient for the function, so we use the asymptotic behaviour, for which we get

$$F_l(k,r) \xrightarrow{r\to\infty} C_l \frac{e^{\pi\gamma/2+\mathrm{i}\sigma_l}(2l+1)!}{2^l\Gamma(l+1+\mathrm{i}\gamma)}\sin(kr - l\pi/2 - \gamma\ln 2kr + \sigma_l), \tag{3.38}$$

where σ_l is the Coulomb phase shift, which may be found by comparing the solution with the free particle case in this regime, and is $\sigma_l = \arg\Gamma(l+1+\mathrm{i}\gamma)$.

Again by analogy with the free particle case, we require that

$$F_l(k,r) \xrightarrow{r\to\infty} \sin(kr - l\pi/2 - \gamma\ln 2kr + \sigma_l), \tag{3.39}$$

which fixes the coefficient C_l at

$$C_l = \frac{2^l e^{-\pi\gamma/2}|\Gamma(l+1+\mathrm{i}\gamma)|}{(2l+1)!}, \tag{3.40}$$

hence the regular spherical Coulomb function is

$$F_l(k,r) = \frac{2^l e^{-\pi\gamma/2}|\Gamma(l+1+\mathrm{i}\gamma)|}{(2l+1)!}e^{\mathrm{i}kr}(kr)^{l+1}_1F_1(l+1+\mathrm{i}\gamma; 2l+2; -2\mathrm{i}kr). \tag{3.41}$$

From here, we may normalize the wave function as in the free particle case to get probability density one in the configuration space, and find the solution

$$\psi(r,\theta,\varphi) = \sum_{l=0}^{\infty}\tilde{C}_l e^{\mathrm{i}kr}k^{l+1}r_1^l F_1(l+1+\mathrm{i}\gamma; 2l+2; -2\mathrm{i}kr)P_l(\cos\theta), \tag{3.42}$$

where the coefficients $\tilde{C}_l$ are obtained by the normalization using the orthogonality of the Legendre polynomials, and are

$$\tilde{C}_l = k^{-1}(2l+1)\mathrm{i}^l e^{\mathrm{i}\sigma_i}C_l. \tag{3.43}$$

Substituting them in the wave function, we have

$$\psi(r,\theta,\varphi) = (kr)^{-1}\sum_{l=0}^{\infty}(2l+1)\mathrm{i}^l e^{\mathrm{i}\sigma_l}F_l(k,r)P_l(\cos\theta). \tag{3.44}$$

We see that this is a complete analog to the plane wave, from which it differs only in the fact that it has $(kr)^{-1}F_l(k,r)$ instead of the usual Bessel $j_l(kr)$.

Since we have produced a parallel for the spherical Bessel functions of the first kind, we will have good use of one for the second kind. We may define the irregular spherical Coulomb function, G_l,

$$G_l(k,r) = C_l e^{\mathrm{i}kr}(kr)^{l+1}G(l+1+\mathrm{i}\gamma;2l+2;-2\mathrm{i}kr), \tag{3.45}$$

where G is another solution (an irregular one) to the Kummer-Laplace equation.

Using the same values for the constants, the function has the asymptotic behaviour

$$G_l(k,r) \xrightarrow{r\to\infty} -\cos(kr - l\pi/2 - \gamma\ln 2kr + \sigma_l). \tag{3.46}$$

Thus, we get the analogy of $n_l(kr)$ to be $(kr)^{-1}G_l(k,r)$.

3.3.3 Coulomb phase shifts

Having built the solution for the Coulomb potential, we will compute the effect of a local central potential on the equation. This way, we now need to consider the radial Schrödinger equation

$$\left[\frac{\mathrm{d}^2}{\mathrm{d}r^2} + k^2 - \frac{2\mu Z_1 Z_2\alpha}{r} - 2\mu\hat{V}(r) - \frac{l(l+1)}{r^2}\right]u_l(r) = 0. \tag{3.47}$$

As the local field vanishes above some R, the solution will be a Coulomb wave for $r > R$, that is

$$u_l(r) = c_l' F_l(k,r) + c_l'' G_l(k,r). \tag{3.48}$$

We may build an analog to the Hankel functions as $H_l^{\pm} = e^{\mp\mathrm{i}\sigma_l}(F_l \pm \mathrm{i}G_l)$. Hence, we rewrite this factorization as

$$u_l(r) = a_l[H_l^-(k,r) + e^{2\mathrm{i}\Delta_l}H_l^+(k,r)]. \tag{3.49}$$

This is useful, because the asymptotic behaviour now becomes

$$u_l(r) \xrightarrow{r\to\infty} \mathrm{i}a_l[e^{-\mathrm{i}(kr-l\pi/2-\gamma\ln 2kr)} - e^{2\mathrm{i}\Delta_l}e^{\mathrm{i}(kr-l\pi/2-\gamma\ln 2kr)}]. \tag{3.50}$$

If the local potential is real, then Δ_l is also real. In the abscence of said local potential, we have $\Delta_l = \sigma_l$, so we write $\Delta_l = \sigma_l + \hat{\delta}_l$. Hence, σ_l is the phase shift due to the Coulomb potential, whereas $\hat{\delta}_l$ is the phase shift due to the local potential with respect to the Coulomb wave.

We may then adapt the same procedure we used for the computation of the phase shift, which will now be

$$\cot\hat{\delta}_l = \frac{kRG_l'(kR) - \beta_l G_l(kR)}{kRF_l'(kR) - \beta_l F_l(kR)}, \tag{3.51}$$

if we write $\beta_l = Ru_l'(R)/u_l(R)$ (the dimensionless logarithmic derivative).

Using the definition of this phase shift, and normalizing the wave so that it behaves as a Coulomb function plus a scattered wave (asymptotically), we get the expression for the reduced radial wave function away at $r > R$,

$$u_l(r) = e^{\mathrm{i}\Delta_l}[\cos\hat{\delta}_l F_l(k,r) - \sin\hat{\delta}_l G_l(k,r)]. \tag{3.52}$$

3.4 $\mathrm{p}\Omega$ scattering

Having developed a way of introducing the Coulomb interaction in our scattering computation, we can tackle the numerical calculation of the $\mathrm{p}\Omega$ scattering. The code developed is completely analogous to the one used for the neutron wave functions (see section A.2).

3.4.1 $p\Omega$ scattering wave functions in the $^5S_2$ channel

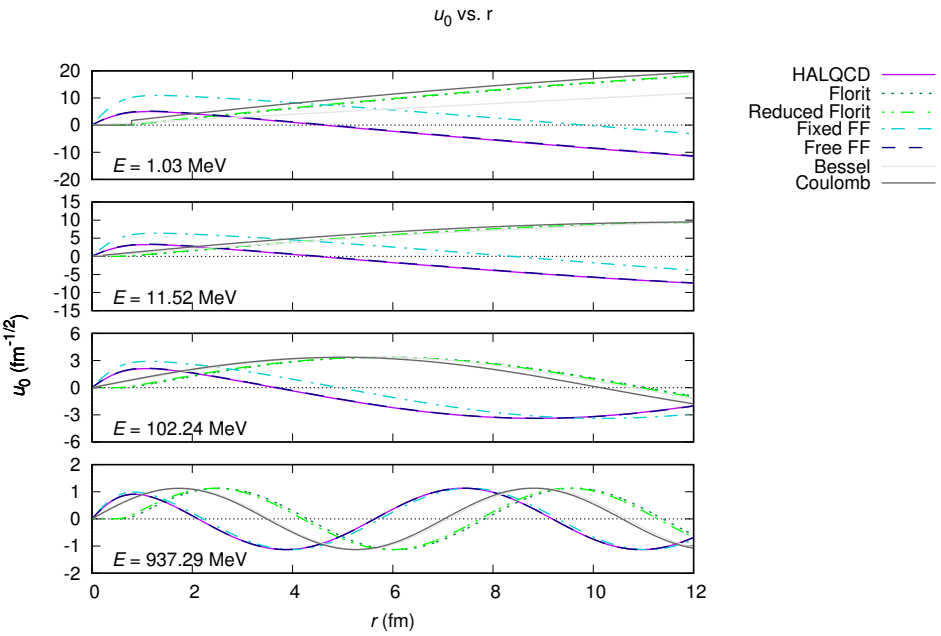

Figure 20: Radial wave functions for various energies, obtained using last section's potentials for the $^5S_2$ $p\Omega$ channel.

We observe, predictably, a qualitatively similar behaviour as the one for the neutron case. This is also reflected on the phase shifts.

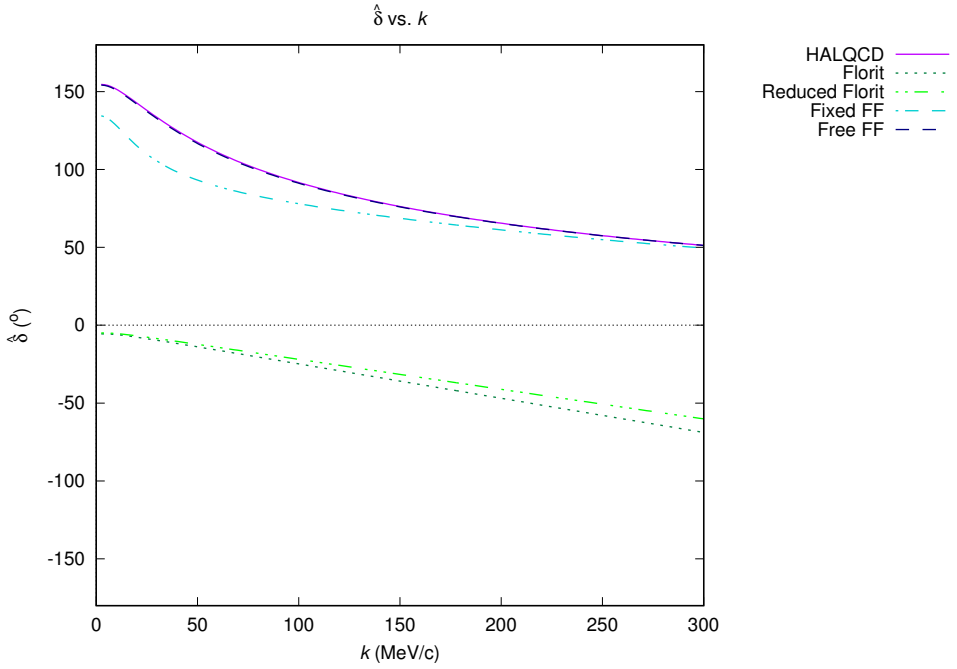

Figure 21: Phase shifts for the $^5S_2$ $p\Omega$ channel, obtained using last section's potentials.

3.4.2 $p\Omega$ scattering wave functions in the $^3S_1$ channel

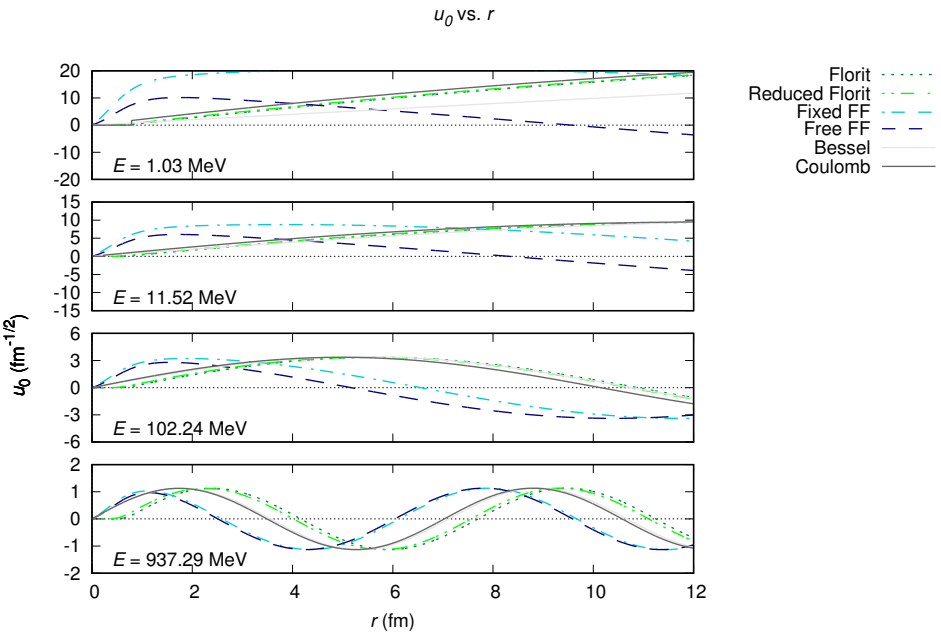

Figure 22: Radial wave functions for various energies, obtained using last section's potentials for the $^3S_1$ $p\Omega$ channel.

Again, we find not much qualitative difference between this case and the proton one. One actual difference is noticeable in the phase shift graph, where we see that the "fixed form factors" fit potential does not have its phase shift starting at zero anymore.

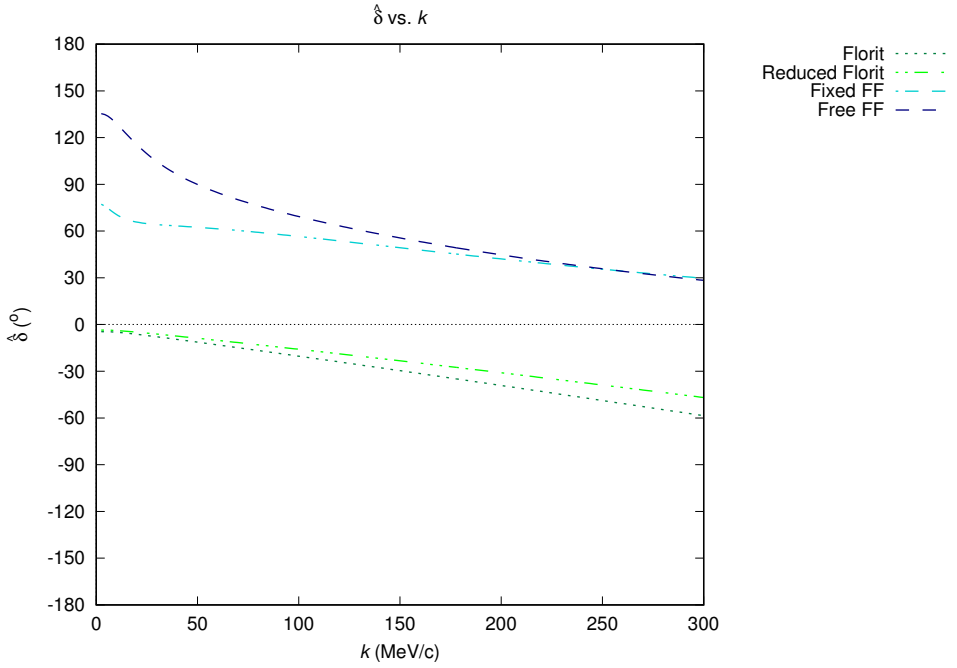

Figure 23: Phase shifts for the $^3S_1$ $p\Omega$ channel, obtained using last section's potentials.

As noted, these phase shifts are quite similar to the non-Coulomb phase shifts. Even if it could seem

like we have not gained much in introducing the Coulomb formalism, it is necessary for the femtoscopy calculation.

4 Femtoscopy of the $N\Omega$ interaction

As mentioned in the introduction, performing scattering experiments with Ω baryons is quite difficult, since it is challenging to produce and maintain a beam of such particles. There is, hence, a need for a different approach [FMV21].

The fundamental quantity studied in femtoscopy is the correlation function, which is expressed in terms of the relative momentum $\vec{k}$. In the center of mass reference frame, it is given by the Koonin-Pratt formula,

$$C(\vec{k}) = \int_{\mathbb{R}^3} S(\vec{r})|\psi(\vec{r},\vec{k})|^2 \,\mathrm{d}\vec{r}\,. \tag{4.1}$$

The first factor in the integrand describes the source which emits the particles, whereas the second factor represents the interaction using the wave function. The source, therefore, is characterized by a scale r_0, which gives a distance scale at which the interacting pairs will be created. This way, the source is a probability density function on $\mathbb{R}^3$.

The interesting thing, however, is the fact that we can also obtain the correlation function directly from experimental results. We obtain it as the fraction of the relative momentum distribution of the pairs produced in the same event N with respect to a reference distribution obtained combining particles produced in different collisions, N_{ref},

$$C_{\mathrm{exp}}(\vec{k}) = \xi(\vec{k})\frac{N(\vec{k})}{N_{\mathrm{ref}}(\vec{k})}. \tag{4.2}$$

ξ represents the corrections due to experimental effects.

This experimental correlation function is distorted by two mechanisms. The pair sample may include not only primary particles but also secondary or wrongly identified particles. This will make some non genuine contributions to the measured correlation function. More details can be found in [FMV21].

4.1 Generalities on correlation functions

The correlation function maps the features present in the interaction. In particular, the effect of the interaction in the final states is more obvious for small values of $\vec{k}$. A repulsive interaction, with positive values of the local potentials, implies that the correlation function will obey $C(\vec{k}) < 1$. Conversely, an attractive interaction will give values of the correlation function with $C(\vec{k}) > 1$.

This intuitive idea, however, changes if the attraction is strong enough to admit a bound state. In this case, the correlation function shows a depletion depending on the binding energy. This is due to the fact that the pairs which form the bound state do not have any effect on the correlation, since they are in a different final state. If the binding energy is strong enough, that is, if the potential is attractive enough, the correlation will show features similar to the repulsive case.

Different sizes of the source can also affect the correlation strength, of course. Resonance, interference and other effects may also appear at different ranges of $\vec{k}$.

The sensibility of the method to study the strong interaction depends on the superposition of the wave function with the source probability distribution function. The useful radii depend on the experiment, but usually lay in the order of magnitude of $r_0 \sim 1\mathrm{fm}$ for pp collisions, for example.

To compute the Koonin-Pratt formula (4.1), in the case of spherically symmetric sources, we may think of performing the integration directly on a partial wave expansion

$$\psi(\vec{r},\vec{k}) = \sum_{l=0}^{\infty} \mathrm{i}^l(2l+1)\frac{u_l(r,k)}{r}P_l(\cos\theta), \tag{4.3}$$

where θ is the polar angle between $\vec{r}$ and $\vec{k}$, and P_l are the Legendre polynomials. Squaring the modulus

of the expansion directly yields

$$\begin{aligned}|\psi(\vec{r},\vec{k})|^2 &= \sum_{l_1=0}^{\infty} \mathrm{i}^{l_1}(2l_1+1)\frac{u_{l_1}(r,k)}{r}P_{l_1}(\cos\theta)\sum_{l_2=0}^{\infty}\mathrm{i}^{-l_2}(2l_2+1)\frac{u_{l_2}(r,k)^*}{r}P_{l_2}(\cos\theta)\\ &= \frac{1}{r^2}\sum_{l=0}^{\infty}(2l+1)^2|u_l(r,k)|^2P_l(\cos\theta)^2\\ &\quad+\frac{2}{r^2}\sum_{l_1=0}^{\infty}\sum_{l_2=l_1+1}^{\infty}(2l_1+1)(2l_2+1)\,\mathrm{Re}[u_{l_1}(r,k)u_{l_2}(r,k)^*]P_{l_1}(\cos\theta)P_{l_2}(\cos\theta).\end{aligned} \tag{4.4}$$

Now, the spherical symmetry of the source means that the fact that $S(\vec{r})$ is a probability density on $\mathbb{R}^3$ is equivalent to $4\pi r^2 S(\vec{r})$ being a probability density on $[0,\infty)$. Therefore, we may integrate this rather messy equation using the orthogonality of the Legendre polynomials, which may be written

$$\int_{-1}^{1} P_n(x)P_m(x)\,\mathrm{d}x = \frac{2}{2n+1}\delta_{nm}, \tag{4.5}$$

as they are now the only non-radial factor left. Hence, all the integrals with respect to $\mathrm{d}\cos\theta$ vanish for the second term, and those on the first term just add a factor. Thus, we get a new expression for the correlation function,

$$C(\vec{k}) = 4\pi\sum_{l=0}^{\infty}(2l+1)\int_0^{\infty}S(r)|u_l(r,k)|^2\,\mathrm{d}r\,. \tag{4.6}$$

However, this expression is rather difficult to compute numerically, and we may find more comfortable approximate forms.

4.1.1 Reduction of the Koonin-Pratt formula for the Coulomb-less case

As for the computation, it is convenient to reduce the Koonin-Pratt formula so that we can calculate a good approximation using only the s-mode of the wave function, again in the case of sources with spherical symmetry.

Without interactions, the wave equation would become a plane wave $\exp(\mathrm{i}\vec{k}\cdot\vec{r})$ and the partial wave modes would be $u_l(r,k) = (2l+1)\mathrm{i}^l j_l(kr)$, where j_l are the Bessel spherical functions of the first kind. This is the idea behind the approximation: we suppose that the interaction affects only the mode with $l=0$ and the modes φ_l with $l\in\{1,2,\dots\}$ remain unaltered, that is, Bessel functions. In this case, since $P_0(x)=1$ by definition, we have

$$\begin{aligned}\psi(\vec{r},\vec{k}) &= \frac{u_0(r,k)}{r}+\sum_{l=1}^{\infty}(2l+1)\mathrm{i}^l j_l(kr)P_l(\cos\theta)\\ &= \frac{u_0(r,k)}{r}-j_0(r,k)+\sum_{l=0}^{\infty}(2l+1)\mathrm{i}^l j_l(kr)P_l(\cos\theta)\\ &= \frac{u_0(r,k)}{r}-j_0(kr)+\exp(\mathrm{i}\vec{k}\cdot\vec{r}),\end{aligned} \tag{4.7}$$

where the last step is just Rayleigh's identity.

To compute the Koonin-Pratt formula (4.1), we need the squared modulus of the wave function, thus

$$\begin{aligned}|\psi(\vec{r},\vec{k})|^2 &= (\mathrm{Re}\,\psi(\vec{r},\vec{k}))^2+(\mathrm{Im}\,\psi(\vec{r},\vec{k}))^2\\ &= (\mathrm{Re}\,u_0(r,k)/r-j_0(kr)+\cos(\vec{k}\cdot\vec{r}))^2+(\mathrm{Im}\,u_0(r,k)/r+\sin(\vec{k}\cdot\vec{r}))^2\\ &= 1+|u_0(r,k)/r|^2+(j_0(kr))^2+2\cos(\vec{k}\cdot\vec{r})\,\mathrm{Re}\,u_0(r,k)/r\\ &\quad+2\sin(\vec{k}\cdot\vec{r})\,\mathrm{Im}\,u_0(r,k)/r-2j_0(kr)\,\mathrm{Re}\,\varphi_0(r,k)/r-2\cos(\vec{k}\cdot\vec{r})j_0(kr).\end{aligned} \tag{4.8}$$

When integrating the expression, we take into account the fact that $\vec{r}\cdot\vec{k} = rk\cos\theta$, so expressing $\vec{r}$ in terms of θ, we get $\mathrm{d}\vec{r} = 2\pi r^2\,\mathrm{d}r\,\mathrm{d}\cos\theta$ (the 2π factor arises from the integration with respect to the other angular component, on which the integrand is invariant). Integrating with respect to $\mathrm{d}\cos\theta$, there will only appear integrals of the three following kinds:

$$\begin{aligned}\int_{-1}^{1}\mathrm{d}\cos\theta &= 2,\\ \int_{-1}^{1}\sin(kr\cos\theta)\,\mathrm{d}\cos\theta &= 0,\\ \int\cos(kr\cos\theta)\,\mathrm{d}\cos\theta &= 2\frac{\sin(kr)}{kr}\\ &= 2j_0(kr);\end{aligned} \tag{4.9}$$

hence, the terms with a sine vanish and the last term of the second last line cancels with the second to last term of the last line. Thus, there only remains

$$\begin{aligned}C(\vec{k}) &= 4\pi\int_0^\infty r^2S(r)[1+|u_0(r,k)/r|^2-(j_0(kr))^2]\,\mathrm{d}r\\ &= 1+4\pi\int_0^\infty S(r)[|u_0(r,k)|^2-(rj_0(kr))^2]\,\mathrm{d}r,\end{aligned} \tag{4.10}$$

where in the last step we used the source normalization.

4.1.2 Reduction of the Koonin-Pratt formula for the Coulomb case

For the Coulomb case, we perform again an expansion of the wave function in partial waves,

$$\psi(\vec{r},\vec{k}) = \sum_{l=0}^{\infty}\mathrm{i}^l(2l+1)\frac{u_l(r,k)}{r}P_l(\cos\theta), \tag{4.11}$$

but in this case, the wave functions without interactions is not a plane wave, but a Coulomb wave. We will again apply the s-wave approximation, and we get

$$\begin{aligned}\psi(\vec{r},\vec{k}) &= \frac{u_0(r,k)}{r}+\sum_{l=1}^{\infty}e^{\mathrm{i}\sigma_l}\mathrm{i}^l\frac{2l+1}{kr}F_l(k,r)P_l(\cos\theta)\\ &= \frac{u_0(r,k)}{r}-e^{\mathrm{i}\sigma_0}\frac{F_0(k,r)}{kr}+\sum_{l=0}^{\infty}e^{\mathrm{i}\sigma_l}\mathrm{i}^l\frac{2l+1}{kr}F_l(k,r)P_l(\cos\theta)\\ &= \frac{u_0(r,k)}{r}-e^{\mathrm{i}\sigma_0}\frac{F_0(k,r)}{kr}+e^{-\pi\gamma/2}\Gamma(1+\mathrm{i}\gamma)e_1^{\mathrm{i}kr\cos\theta}F_1(-\mathrm{i}\gamma;1;\mathrm{i}kr(1-\cos\theta)),\end{aligned} \tag{4.12}$$

where γ is the Sommerfeld parameter.

We'll label the last term ψ_c, for simplicity purposes. In this case, the difference lays in the fact that the wave function is not modulus one in general, and its real and imaginary parts are not so simple. For the squared modulus, we get

$$\begin{aligned}|\psi(\vec{r},\vec{k})|^2 &= (\operatorname{Re}\psi(\vec{r},\vec{k}))^2+(\operatorname{Im}\psi(\vec{r},\vec{k}))^2\\ &= |\psi_\mathrm{c}(r,k)|^2+|u_0(r,k)/r|^2+|F_0(k,r)/kr|^2+2\operatorname{Re}\psi_\mathrm{c}(\vec{r},\vec{k})\operatorname{Re}u_0(r,k)/r\\ &\quad+2\operatorname{Im}\psi_\mathrm{c}(\vec{r},\vec{k})\operatorname{Im}u_0(r,k)/r-2\cos\sigma_0\operatorname{Re}F_0(k,r)[\operatorname{Re}u_0(r,k)/r+\operatorname{Re}\psi_\mathrm{c}(\vec{r},\vec{k})]/kr\\ &\quad-2\sin\sigma_0\operatorname{Im}F_0(k,r)[\operatorname{Im}u_0(r,k)/r+\operatorname{Im}\psi_\mathrm{c}(\vec{r},\vec{k})]/kr.\end{aligned} \tag{4.13}$$

Under angular integration, all terms in the expansion of $\psi_{\rm c}$ vanish except for the $l = 0$ one will vanish due to the ortogonality of the Legendre polynomials. The remaining term can be cancelled with the other factors and we get a similar reduction for the Koonin-Pratt formula (4.1),

$$\begin{aligned} C(\vec{k}) &= \int_{\mathbb{R}^3} S(r)|\psi_{\rm c}(\vec{r},\vec{k})|^2\,{\rm d}\vec{r} + 4\pi\int_0^\infty S(r)[|u_0(r,k)|^2 - |F_0(k,r)/k|^2]\,{\rm d}r \\ &= 2\pi e^{-\pi\gamma}|\Gamma(1+{\rm i}\gamma)|^2\int_{-1}^{1}{\rm d}\cos\theta\int_0^\infty r^2 S(r)|{}_1F_1(-{\rm i}\gamma;1;{\rm i}kr(1-\cos\theta))|^2\,{\rm d}r \\ &\quad + 4\pi\int_0^\infty S(r)[|u_0(r,k)|^2 - |F_0(k,r)/k|^2]\,{\rm d}r\,. \end{aligned} \tag{4.14}$$

4.2 $N\Omega$ interaction correlation functions

Having developed the correlation function formalism, it is time to obtain the correlation functions for the $N\Omega$ pair. To do so, we have to consider the fact that we are operating on multiple interaction channels. In particular, we have considered the $L = L' = 0$ channels,

$$\begin{aligned} {}^3S_1 &\to {}^3S_1, \\ {}^5S_2 &\to {}^5S_2. \end{aligned} \tag{4.15}$$

Making an equiprobability assumption in the creation of the pair, and taking into account each state's degeneracy, we compute a spin-weighted sum,

$$C(\vec{k}) = \frac{3C({}^3S_1;\vec{k}) + 5C({}^5S_2;\vec{k})}{8}, \tag{4.16}$$

where we have labeled each channel correlation function with the state's ${}^{2S+1}L_J$ label.

For a source function, since we want to compare the pΩ results with the pp collision ones in [ALI20], we will use the one used there, that is, a Gaussian

$$S(\vec{r}) = (4\pi {r_0}^2)^{-3/2} e^{-(r/2r_0)^2}, \tag{4.17}$$

with $r_0 = 0.95$ fm.

As for each of the correlation functions, we have obtained them again through a Fortran 90 code (see section A.2).

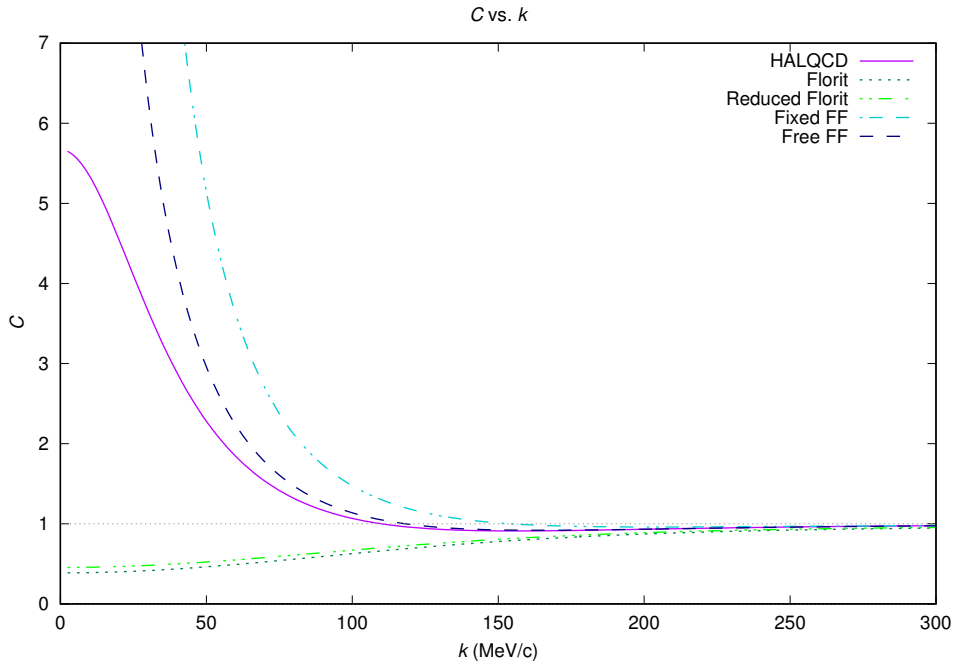

Figure 24: Correlation functions for the developed potentials, for the $n\Omega$ interaction.

For the neutron case, we see that the interactions with a strong attractive behaviour (all except the Florit parametrizations) are above one nearly everywere. However, all of them do cross the one line at some point, which is to be expected as they all have bound states in at least one channel. Meanwhile, the repulsive interactions (the Florit parametrizations) stay below one throughout all of the domain.

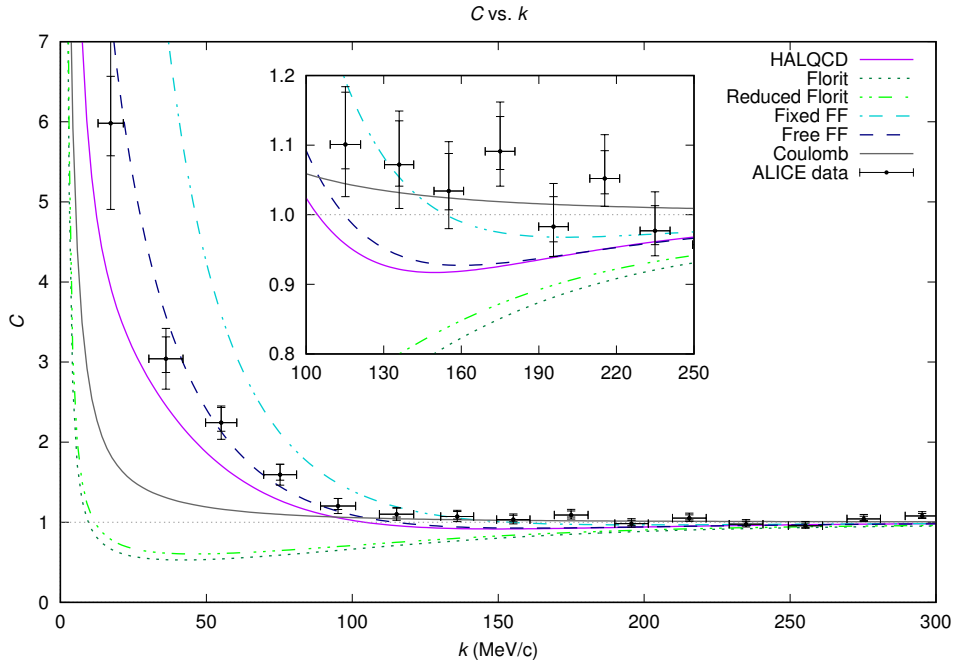

Figure 25: Correlation functions for the developed potentials, for the $p\Omega$ interaction including the Coulomb interaction, together with ALICE data from [ALI20].

The proton case is a bit complicated due to the fact that the Coulomb interaction naturally generates a rise in the correlation values for small k. This slightly complicates things, as very different interactions yield qualitatively similar results. In particular, the very repulsive Florit parametrizations now show a

very similar behaviour (although sharper) to the attractive interactions considered.

The interesting thing to see here, however, is the comparison with the ALICE data. As we can see, the free FF potential is the one that more closely follows the ALICE data in large sectors of the studied range. Adding the ${}^3S_1$ has, therefore, proven to raise the values of the correlation function so that they are closer to the data. At low momenta we even find a small overestimation of the data.

We observe, for both FF potentials as well as the HAL QCD potential, a dip in the region between $100\ \mathrm{MeV/c}$ and $200\ \mathrm{MeV/c}$. This depletion corresponds to the bound state we computed in the first section, and is not observed in the [ALI20] data.

We must remember that we have left some contributions out of the calculation. In particular, we have not considered any strangeness rearrangement nor the inelastic channels coupling to $L' = 2$ modes or higher L modes. This channels, according to the conclusions in [ALI20], are dominated by absorption and should be neglected. However, the rising in the values due to the addition of the ${}^3S_1$ channel leaves some room to improve the description with the inelastic channels.

Therefore, we may conclude that the not yet considered channels (that is, the coupled channels and the higher partial waves) may indeed provide a non-negligible contribution to the correlation function.

5 Summary, conclusions and outlook

In this work, we wished to study the baryon-baryon $p\Omega$ interaction. Since there is no scattering measurements for this interaction, we used the femtoscopy method, which gives information on the interaction at microscopic level.

We have derived a potential for the strong $N\Omega$ interaction using an effective field theory up to LO taking into account the contributions from contact terms, an η exchange term and a σ exchange term. This potential has five free parameters, with which we have fitted the ${}^5S_2 \to {}^5S_2$ channel to the known $p\Omega$ lattice QCD strong potential obtained by the HAL QCD collaboration.

This process has yielded different parameter sets for the potential. In particular, we have developed a fitting without form factors (which has yielded poor results and we have disregarded), a fit where we fixed the form factors to physically reasonable values and fit the rest of the parameters (which we called "fixed form factors" parametrization), and one where we fit with all the parameters (which we called "free form factors" parametrization). Additionally, we have considered two parametrizations from a previous work [Flo14] which did not consider neither form factors nor the σ exchange term (which we called Florit parametrizations).

These parametrizations, along with the effective potential expression, allowed us to obtain the potential for the ${}^3S_1 \to {}^3S_1$ channel. Although not included in this work, the effective potential derivation has also yielded a tensor term responsible for the inelastic channels with $L' = 2$.

The "free form factors" fit has shown very good accordance with the HAL QCD potential and its bound states, scattering wave functions and correlation functions, even though it has given a low value for the σ exchange form factor. The other fits have also shown good accordance at some regions but have proven unable to reproduce both its behaviour and extracted results.

The Florit parametrizations, in particular, does not reproduce the HAL QCD potential attractiveness, but have proven useful through the work to study a very repulsive limiting case for the potential.

In regards to the bound states, for the parametrizations of this potential including form factors, we have found not only the already suspected ${}^5S_2$ bound state for $p\Omega$ and $n\Omega$, but also a ${}^3S_1$ bound state for $p\Omega$. This seems to reinforce the hypothesis that the $p\Omega$ interaction is able to generate a bound dibaryon, even though it still has not been found experimentally.

Using the parametrizations obtained in this work, we have computed numerically the scattering wave functions for the s-wave. These have shown phase shifts which are in accordance with the mentioned bound states through Levinson's theorem. As expected, the "free form factors" fit does reproduce very well the HAL QCD potential results for the scattering, whereas the results for the rest of the parametrizations were much less successful.

In particular, for the Florit parametrizations' wave functions we can observe the very repulsive core as a constant-like behaviour of the scattering wave functions for very small radii.

We have computed the femtoscopy correlation function by using the Koonin-Pratt formula with the scattering wave functions computed previously, for both $n\Omega$ and $p\Omega$ pairs, using the different parametrizations.

We have seen that the "free form factors" fit slightly improves on the HAL QCD potential in following the [ALI20] $p\Omega$ data, even overestimating it at some energy values. In particular, the fact that the correlation function is slightly increased by adding the ${}^3S_1$ potential leaves some space for the coupled channels to give a slight negative contribution.

This fact leads us to think that, given that the higher partial waves will contribute positively to the correlation function, the inelastic channels may provide a negative contribution to compensate, at least partly, said overestimation. Therefore, we conclude that the coupled channels may have a non negligible effect on the function.

All of the numerical computations have been done using Fortran 90 programs built from scratch (save for subroutines for the gamma, Bessel, Coulomb and confluent hypergeometric functions) using known methods. In particular, we have made extensive use of the Numerov discretization, the shooting method and the trapezoidal rule.

The exception to this are the fittings of the potential, which have been obtained using a Python script to perform a minimum squares fitting.

At the moment, work is being done both in obtaining the errors in the potential fits and their χ^2 value in order to obtain a quantitative estimation of their goodness. We are also working in trying to propagate the errors on the fits to the observables obtained from them. In particular, to the correlation function results.

One direct extension for this work would be the comparison of our correlation functions with those of the Lednický-Lyuboshitz model, for which we would need to compute the low-energy scattering parameters, to test its validity. Systematic analyses on the source function and dependence on the Gaussian radius would also provide relevant information.

Further work on this project should include not only the computation of higher partial waves, but also the inelastic channels. Even though a first step in this direction is relatively easy, since we have already computed the tensor components of our potential coupling to $L' = 2$, this will not be a trivial task, since it will need adapting the numerical method for solving the matrix system of coupled Schrödinger equations.

Another direction in which one could continue the work would involve extending the effective field theory to next-leading-order, which would add new contributions to the interaction.

One could also use this work to study other baryon-baryon systems already incorporated in our formalism, like the $\mathrm{p}\Xi^-$ system.

A Appendix: Code description

The codes we used for the work have been developed using the Fortran 90 language, aided by subroutines and functions we used to compute special functions, namely, the Bessel, Coulomb, Gamma and confluent hypergeometric function.

A.1 Bound states

The code developed to find the bound states takes a potential function V, a range R which should be taken to be very far where the potential is no longer relevant, a matching point $R^* < R$ which should be taken to be at some point where the potential is still relevant but has already began to decay, a number N of nodes to discretize the space and a small tolerance $\varepsilon \in \mathbb{R}^+$.

First of all, the code discretizes the $[0, R]$ range with spacing $\Delta R = R/N$, so we have a grid $\{r_0, \ldots, r_N\}$ with $r_i = i\Delta R$ and the matching point is now r_M, where $M = \lfloor NR^*/R \rfloor$. We write $V_i = V(r_i)$ and $u_i = u(r_i)$ for the potential and radial wave functions, with $i \in \{0, \ldots, N\}$. Next, we set $E^+ = 0$ and $E^- = V(r_0)$.

Now the code will iterate a bisection process. We take $E = (E^+ + E^-)/2$ and use the Numerov discretization to solve eq. (3.32). Numerov's formula, applied to the radial Schrödinger equation, is written [Gia21]

$$u_{i+2} = \frac{(12 - 10f_{i+1})u_{i+1} - f_i u_i}{f_{i+2}}, \tag{A.1}$$

where

$$f_i = 1 + \frac{\mu}{6}\left(\frac{\Delta R}{\hbar}\right)^2 [E - V_i]. \tag{A.2}$$

We set $u_0 = 0$, $u_1 = (\Delta R)^{l+1}$ and iterate the formula until we obtain u_M.

Opposite, we set $u_N = 0$, $u_{N-1} = (\Delta R)^{l+1}$ and apply Numerov's formula backwards,

$$u_{i-2} = \frac{(12 - 10f_{i-1})u_{i-1} - f_i u_i}{f_{i-2}}, \tag{A.3}$$

until we obtain a different value for u_M, which we call u_M^*. We then multiply $u_{M+1}, \ldots, u_N$ by u_M/u_M^*, so that the function is properly scaled.

Now, we compute the forward derivative at M, $u_M'^F$, and the backward derivative at M, $u_M'^B$. Now, if $u_M'^F - u_M'^B > 0$, the energy chosen is too high and we redefine $E^+ = E$. On the contrary, if $u_M'^F - u_M'^B < 0$, the energy chosen is too low and we redefine $E^- = E$.

We repeat this process until $E^+ - E^- < \varepsilon$. Once this happens, the desired energy is at the center of the interval, $E = (E^+ + E^-)/2$. We normalize the state by integrating ${u_i}^2$from r_0 to r_N using the trapezoidal rule,

$$N = \left[\frac{{u_0}^2 + {u_N}^2}{2} + \sum_{i=1}^{N-1} {u_i}^2\right]\Delta R \tag{A.4}$$

and dividing all u_i by $\sqrt{N}$.

Now, we obtain the mean squared radius of the state by integrating ${u_i}^2{r_i}^2$ from r_0 to r_N and taking the square root of the result,

$$\sqrt{\langle r^2 \rangle} = \sqrt{\left[\frac{{u_0}^2{r_0}^2 + {u_N}^2{r_N}^2}{2} + \sum_{i=1}^{N-1} {u_i}^2{r_i}^2\right]\Delta R}.$$

A.2 Scattering states and correlation functions

The code developed to find the scattering states and correlation functions takes a potential function V, a range R which should be taken to be very far where the potential is no longer relevant, a number N_E of energy values to compute, energies $E_0 \in \mathbb{R}^+$ and $E_{N_E} > E_0$ which are the lowest and highest the code will compute, and numbers N_θ and N_r which will serve to discretize the correlation function integrals. These last two numbers are only needed for the Coulomb case (that is, the pΩ case).

In order to get the momenta to be linearly spaced, we define the energy levels $E_1, \dots, E_{N_E-1}$ as

$$E_i = E_1 + \left(\frac{i}{N}\right)^2 (E_{N_E} - E_1),$$

instead of just organizing them linearly. For each of these energy levels, we proceed with the following calculations. We define the momenta $k_i = \sqrt{2\mu E_i}$ and the values of the correlation function $C_i = C(k_i)$.

As did in the previous code, we discretize the $[0, R]$ range with spacing $\Delta R = R/N$, so we have a grid $\{r_0, \dots, r_N\}$ with $r_i = i\Delta R$. We write $V_i = V(r_i)$ and $u_i = u(r_i)$ for the potential and radial wave functions, with $i \in \{0, \dots, N\}$.

For a certain energy level E_j, then, we set $u_0 = 0$ and $u_1 = \Delta R$. We then apply Numerov's formula (A.1) to obtain $u_2, \dots, u_N$. We have the scattering state, but we need to scale it. To do so, we compute the logarithmic derivative at point N, β_0, as

$$\begin{aligned} \beta_0 &= \frac{3u_N - 4u_{N-1} + u_{N-2}}{2\Delta R u_N} r_N \\ &= \frac{3u_N - 4u_{N-1} + u_{N-2}}{2u_N} N. \end{aligned} \tag{A.5}$$

Using it, we obtain the phase shift of the state with eq. (3.21) for the non Coulomb case, and eq. (3.51) for the Coulomb case. For the first case, we need the Bessel and Von Neumann function, which we compute with subroutines from [ZJ96]. For the second case, we need the Coulomb functions, which we compute with subroutines from [SF19].

Using these phase shifts, we compute the "true" value of the wave function u_N, which we label u_N^*, with eq. (3.20) or eq. (3.52), respectively. We set the global phase so that the value is real. Then, we multiply $u_0, \dots, u_N$ by u_N^*/u_N.

Now we already have the E_j scattering state. We can now compute the correlation function value C_j. To do so, we use eq. (4.10) for the non Coulomb case, which requires integrating by the trapezoidal rule,

$$C_j = 1 + 4\pi \left[\frac{S(r_N)[{u_N}^2 - (r_N j_0(k_j r_0))^2]}{2} + \sum_{i=1}^{N-1} S(r_i)[{u_i}^2 - (r_i j_0(k_j r_i))^2] \right] \Delta R, \tag{A.6}$$

whereas for the Coulomb case the integrals from eq. (4.14) are a bit more cumbersome. Reminding that we are using a Gaussian source S with radius $r_0 = 0.95$ fm (as in eq. (4.17)), we have

$$\begin{aligned} C_j =& 2\pi e^{-\pi\gamma_j} |\Gamma(1 + \mathrm{i}\gamma_j)|^2 I_j \\ &+ 4\pi \left[\frac{S(r_N)[{u_N}^2 - (F_0(k_j, r_0)/k_j)^2]}{2} + \sum_{i=1}^{N-1} S(r_i)[{u_i}^2 - (F_0(k_j, r_i))^2] \right] \Delta R, \end{aligned} \tag{A.7}$$

where γ_j is the Sommerfeld factor for energy E_j and I_j is a the double integral which comes from integrating the confluent hypergeometric function. This one is computed by double trapezoidal integrating

as follows, by defining $\rho_k = kR/N_r$ and $x_i = -1 + 2k/N_\theta$ and adding

$$\begin{aligned} I_j =& \frac{{\rho_{N_r}}^2 S(\rho_{N_r})}{4}\Big[|{}_1F_1(-\mathrm{i}\gamma_j;1;0)|^2 + |\,{}_1\mathrm{F}_1(-\mathrm{i}\gamma_j;1;2\mathrm{i}k_j\rho_{N_r})|^2 \\ &+ 2\sum_{i=1}^{N_\theta-1}|{}_1F_1(-\mathrm{i}\gamma_j;1;\mathrm{i}k_j\rho_k(1-x_i))|^2\Big]\Delta R \\ &+ \sum_{k=1}^{N_r-1}\frac{{\rho_k}^2 S(\rho_k)}{2}\Big[|{}_1F_1(-\mathrm{i}\gamma_j;1;0)|^2 + |\,{}_1\mathrm{F}_1(-\mathrm{i}\gamma_j;1;2\mathrm{i}k_j\rho_k)|^2 \\ &+ 2\sum_{k=1}^{N_r-1}|{}_1F_1(-\mathrm{i}\gamma_j;1;\mathrm{i}k_j\rho_k(1-x_i))|^2\Big]\Delta R \end{aligned} \tag{A.8}$$

We use subroutines from [Mor14] for the gamma function and from [NPB92] for the confluent hypergeometric function.

Note that, for this code, the Bessel functions are actually not needed, since we are staying at $l = 0$. However, we have deemed it convenient to include them so that parts of the code are more easily extendable to other relative angular momenta.

References

[ALI20] ALICE collaboration. "Unveiling the strong interaction among hadrons at the LHC". *Nature* **588**: 232-238 (2020).

[BSS93] M. N. Butler, M. J. Savage and R. P. Springer. "Strong and electromagnetic decays of the baryon decuplet". *Nucl. Phys. B* **399**: 69 (1993).

[Flo14] M. Florit Gual. *Strong baryon-baryon interaction in the strangeness -3 sector* (master's thesis, Universitat de Barcelona, 2014).

[FMV21] L. Fabbietti, V. Mantovani Sarti and O. Vázquez Doce. "Study of the Strong Interaction Among Hadrons with Correlations at the LHC". *Annu. Rev. Nucl. Part. Sci.* **71**: 377-402 (2021).

[Gia21] P. Giannozzi. "Numerical methods in quantum mechanics" (homonymous course class notes, Interateneo Triste – Udine, 2021).

[HP+13] J. Haidenbauer, S. Petschauer et al. "Hyperon-nucleon interaction at the next-to-leading order in chiral effective field theory". *Nucl. Phys. A* **915**: 24-58 (2013).

[IA+19] T. Iritani, S. Aoki et al. "$N\Omega$ dibaryon from lattice QCD near the physical point". *Phys. Lett. B* **792**: 284-289 (2019).

[JM91] E. Jenkins and A. V. Manohar. "Chiral corrections to the baryon axial currents". *Phys. Lett. B* **259**: 353-358 (1991).

[Joa75] C. J. Joachain. *Quantum Collision Theory* (North-Holland Publishing Company, Amsterdam, 1975).

[JOR02] D. Jido, E. Oset and À. Ramos. "Chiral dynamics of the p-wave in $\mathrm{K}^{-}\mathrm{p}$ and coupled states". *Phys. Rev. C* **66**: 055203 (2002).

[LS96] W. Lucha and F. F. Schöberl. "Effective potential models for hadrons". arXiv:hep-ph/9601263 (1996).

[Mac85] R. Machleidt. "The Meson Theory of Nuclear Forces and Nuclear Matter", in *Relativistic Dynamics and Quark-Nuclear Physics: Proc. Los Alamos Workshop*, eds. M. B. Johnson and A. Piclesimer (John Wiley & Sons, New York, 1986).

[Mor14] J.-P. Moreau. "Fortran Routines for Computation of Special Functions" (2014).

[MM23] M. Macêdo-Lima and L. Madeira. "Scattering length and effective range of microscopic two-body potentials". arXiv:2303.04591v2 [quant-ph] (2023).

[NPB92] M. Nardin, W. F. Perger and A. Bhalla. "Solution to the confluent hypergeometric function". *Trans. on Math. Soft.* **18**: 345-349 (1992).

[OR97] E. Oset and À. Ramos. "Nonperturbative chiral approach to s wave $\bar{\mathrm{K}}N$ interactions". *Nucl. Phys. A* **635**: 92-120 (1998).

[Pic95] A. Pich. "Chiral perturbation theory". *Rept. Prog. Phys.* **58**: 563-610 (1995).

[Piq24] M. Piquer i Méndez. "Master's thesis plot data" (GitHub repository, https://github.com/Marc-PiM/Masters_thesis_plot_data, 2024).

[PHM07] H. Polinder, J. Haidenbauer and U.-G. Meißner. "Strangeness $S = -2$ baryon-baryon interactions using chiral effective field theory". *Phys. Lett. B* **653**: 29-37 (2007).

[SD+21] T. R. Saito, W. Dou et al. “New directions in hypernuclear physics”. *Nat. Rev. Phys.* **3**: 803-813 (2021).

[SF19] F. Salvat and J. M. Fernández-Varea. “RADIAL: a Fortran subroutine package for the solution of the radial Schrödinger and Dirac wave equations”. *Comp. Phys. Comm.* **240**: 165-177 (2019).

[SKH18] T. Sekihara, Y. Kamiya and T. Hyodo. “$N\Omega$ interaction: meson exchanges, inelastic channels, and quasibound state”. *Phys. Rev. C* **98**: 015205 (2018).

[Spr99] R. P. Springer. “Heavy barion chiral perturbation theory and the weak nonleptonic p-wave decays of the baryon octet”. *Phys. Lett. B* **461**: 167 (1999).

[ST20] E. Shuryak and J. Torres-Rincon. “Baryon preclustering at the freeze-out of heavy-ion collisions and light-nuclei production”. *Phys. Rev. C* **101**: 034914 (2020).

[STA19] STAR collaboration. “The proton-Ω correlation function in $\mathrm{Au}+\mathrm{Au}$ collisions at $\sqrt{s_{\mathrm{NN}}}=200\mathrm{GeV}$”. *Phys. Lett. B* **790**: 490-497 (2019).

[TF20] L. Tolós and L. Fabbietti. “Strangeness in nuclei and neutron stars”. *Prog. Part. Nucl. Phys.* **112**: 103770 (2020).

[Tor23] J. Torres-Rincon. Private notes.

[SW86] B. D. Serot and J. D. Walecka. “The Relativistic Nuclear Many Body Problem”. *Adv. Nucl. Phys.* **16**: 1-327 (1986).

[Wei90] S. Weinberg. “Nuclear forces from chiral lagrangians”. *Phys. Lett. B* **251**: 288-292 (1990).

[Zho06] Zhong-Qi M. “The Levinson theorem”. *J. Phys. A Math. Gen.* **39**: R625-R659 (2006).

[ZJ96] S. Zhang and J. Jin. *Computation of special functions* (John Wiley & Sons, Hoboken, 1996).